INTERNATIONAL JOURNAL FOR NUMERICAL METHODS IN FLUIDS
Int. J. Numer. Meth. Fluids 2009; **59**:711–751
Published online 20 August 2008 in Wiley InterScience (www.interscience.wiley.com). DOI: 10.1002/fld.1809

Applications of the dual integral formulation in conjunction with fast multipole method to the oblique incident wave problem

K. H. Chen[1], J. T. Chen[2,*,†], J. H. Kao[3] and Y. T. Lee[2]

[1]*Department of Civil Engineering, National Ilan University, Ilan 26047, Taiwan*
[2]*Department of Harbor and River Engineering, National Taiwan Ocean University, Keelung 20224, Taiwan*
[3]*Department of Hydraulic and Ocean Engineering, National Cheng Kung University, Tainan 70101, Taiwan*

SUMMARY

In this paper, the dual integral formulation is derived for the modified Helmholtz equation in the propagation of oblique incident wave passing a thin barrier (zero thickness) by employing the concept of fast multipole method (FMM) to accelerate the construction of an influence matrix. By adopting the addition theorem, the four kernels in the dual formulation are expanded into degenerate kernels that separate the field point and the source point. The source point matrices decomposed in the four influence matrices are similar to each other or only to some combinations. There are many zeros or the same influence coefficients in the field point matrices decomposed in the four influence matrices, which can avoid calculating the same terms repeatedly. The separable technique reduces the number of floating-point operations from $O((N)^2)$ to $O(N\log^a(N))$, where N is the number of elements and a is a small constant independent of N. Finally, the FMM is shown to reduce the CPU time and memory requirement, thus enabling us to apply boundary element method (BEM) to solve water scattering problems efficiently. Two-moment FMM formulation was found to be sufficient for convergence in the singular equation. The results are compared well with those of conventional BEM and analytical solutions and show the accuracy and efficiency of the FMM.

Received 29 August 2006; Revised 22 February 2008; Accepted 23 February 2008

KEY WORDS: fast multipole method; oblique incident wave; thin barrier; modified Helmholtz equation; dual boundary element method; hypersingular equation; divergent series

*Correspondence to: J. T. Chen, Department of Harbor and River Engineering, National Taiwan Ocean University, Keelung 20224, Taiwan.
†E-mail: jtchen@mail.ntou.edu.tw

Contract/grant sponsor: National Science Council; contract/grant number: NSC 95-2221-E-197-026-MY3

1. INTRODUCTION

The boundary element method (BEM), sometimes referred to as the boundary integral equation method (BIEM), is now establishing a position as an actual alternative to the finite element method (FEM) in many fields of engineering. It is necessary to discretize only the boundary instead of the domain, which takes a lesser time for one-dimensional reduction in mesh generation. The dual BEM (DBEM), or so-called the dual BIEM developed by Chen and Hong [1], is particularly suitable for the problems with a degenerate boundary. The dual formulation also plays important roles in some other problems, e.g. the corner problem [2], adaptive BEM [3], the spurious eigenvalue of interior problem [4], the fictitious frequency of exterior problem [5] and the degenerate scale problem [6]. The thin water barrier considered in the present paper is a case of degenerate boundary [7, 8].

Prediction of wave interactions has been studied previously by a number of authors for many kinds of configurations of a water barrier on the basis of linear wave diffraction theory [9–11]. Many analytical and numerical solutions have been developed on the basis of the eigenfunction expansion method [12–16] and the BEM [17–21], respectively. The reflection and transmission of oblique incident water wave past a submerged barrier with a finite width were studied using the conventional BEM under the linear wave theory [18]. In these references, incident angle of the wave, shape of the barrier, barrier height, width and slope under various wave conditions have been considered. Nowadays, submerged breakwaters are often constructed to protect a harbor from waves of the open sea. The primary function is to reduce the wave energy transmitted through it and to have the advantages of allowing water circulation, fish passage and providing economical protection. A suitable arrangement of a thin barrier may act as a good model for a breakwater. The effect of such an arrangement on incident wave can be studied by using the dual BEM, assuming linear theory for the thin breakwater.

There is considerable interest in many applications such as exterior acoustics, Stokes flows, molecular dynamics and electromagnetic-wave problems, when the wave length is short or the wave number is large after comparing with the size of the boundary. The complexity proportional to the conventional BEM is N^2, but the FEM is N because of its banded coefficient matrix [22]. Multi-domain approach [23] or approximate theories such as the theories of plates and shells have been employed to solve the problem using parallel computers. When the size of the influence matrix by using BEM is so large, its storage and solution may cause problems for desktop computer. Thus, the size of the influence matrix becomes the limiting factor that the problems can be solved only with a particular computer. The BEM with iterative solvers has been employed to deal with the problem [24]. The major computational cost of the iterative methods lies in the matrix–vector multiplication. To improve the efficiency in numerical computation of the dual BEM, we will adopt the fast multipole method (FMM) to accelerate the speed of calculation of the four influence matrices.

The FMM was initially introduced by Rokhlin [25, 26] and extended to the Stokes flow field [27]. Applications of FMM for the BEM analysis have been made by many researchers in various fields of science and engineering [22, 27–37]. We will adopt the concept of the FMM to accelerate the calculation of the influence matrix in the dual BEM. By adopting the addition theorem, the four kernels in the dual formulation will be expanded into degenerate kernels where the field point and the source point are separated. The separable technique can promote the efficiency in determining the coefficients. The source point matrices decomposed in the four influence matrices are similar to each other or only to some combinations. There are many zeros or the same influence coefficients in the field point matrices decomposed in the four influence matrices. Therefore, we can avoid

DOI: 10.1002/fld

calculating the same terms repeatedly. The separable technique reduces the number of floating-point operations from $O((N)^2)$ to $O(N\log^a(N))$, where a is a small constant. To accelerate the convergence in constructing the influence matrix, the center of multipole is designed to locate on the center of each boundary element. The singular and hypersingular integrals are transformed into the summability of divergent series and regular integrals. Successful application to acoustic wave was published [37].

In this paper, the problems of oblique incident wave passing a 'thin' water barrier will be considered. Physically speaking, there is no zero thickness breakwater in the real world. However, a finite thickness can be modelled as a zero thickness mathematically after comparing the wave length with the thickness of the breakwater. Dual integral formulation in conjunction with FMM will be used to solve the degenerate boundary problems of oblique incident wave passing a thin barrier. Finally, the CPU time and memory requirement will be calculated using the FMM for the scattering problem of water wave. The numerical results will be compared with those of conventional DBEM and analytical solutions.

2. MATHEMATICAL FORMULATION

2.1. Modified Helmholtz equation in the scattering wave problem with a thin water barrier

Consider a vertical thin barrier parallel to the z-axis as shown in Figure 1. A wave train with a frequency σ propagates towards the barrier with an angle θ in a constant water depth h. Assuming inviscid, incompressible fluid and irrotational flow, the wave field may be represented by the

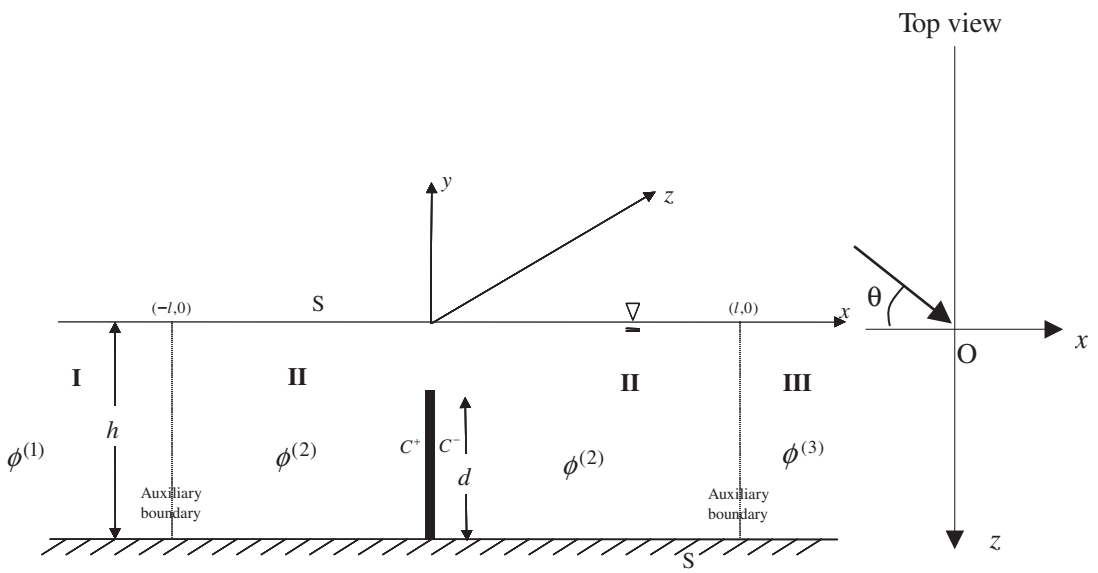

Figure 1. Definition sketch of the water scattering problem of oblique incident wave past a rigid thin barrier.

DOI: 10.1002/fld

velocity potential $\Phi(x, y, z, t)$, which satisfies the Laplace equation as

$$\nabla^2\Phi(x, y, z, t)=0 \tag{1}$$

According to the uniformity of the water depth in the z-axis and the periodicity in time, the potential $\Phi(x, y, z, t)$ of fluid motion can be expressed as

$$\Phi(x, y, z, t)=\phi(x, y)\mathrm{e}^{\mathrm{i}(\lambda z-\sigma t)} \tag{2}$$

where $\lambda=k\sin(\theta)$ and k is the wave number that satisfies the dispersion relation

$$\sigma^2=gk\tanh(kh) \tag{3}$$

in which g is the acceleration of gravity. The unknown function, $\phi(x, y)$, describes the fluctuation of the potential on the xy plane. Substitution of Equations (2) into (1) yields the modified Helmholtz equation as follows:

$$\nabla^2\phi(x, y)-\lambda^2\phi(x, y)=0, \quad (x, y) \text{ in } D \tag{4}$$

where D is the domain of interest. The boundary conditions of the interested domain are summarized as follows:

1. The linearized free water surface boundary condition:

$$\frac{\partial\phi}{\partial y}-\frac{\sigma^2\phi}{g}=0 \tag{5}$$

2. Seabed and breakwater boundary conditions:

$$\frac{\partial\phi}{\partial n}=0 \tag{6}$$

   where n is the boundary normal vector.
3. Radiation condition at infinity:

$$\lim_{x\to\infty} x^{1/2}\left(\frac{\partial\phi}{\partial x}-\mathrm{i}k\phi\right)=0, \quad x \text{ at infinity} \tag{7}$$

4. The boundary conditions on the fictitious interfaces: For the infinite strip problem, the domain can be divided into three regions after introducing two pseudo-boundaries on both sides of the barrier, $x=\pm l$, as shown in Figure 1. The potential in region I without energy loss can be expressed as

$$\phi^{(1)}(x, y)=(\mathrm{e}^{\mathrm{i}\eta(x+l)}+R\mathrm{e}^{-\mathrm{i}\eta(x+l)})\frac{\cosh(k(h+y))}{\cosh(kh)} \tag{8}$$

   where the superscript of ϕ denotes the region number, R is the reflection coefficient and $\eta=k\cos(\theta)$. The potential in region III without energy loss can be expressed by

$$\phi^{(3)}(x, y)=T\mathrm{e}^{\mathrm{i}\eta(x-l)}\frac{\cosh(k(h+y))}{\cosh(kh)} \tag{9}$$

   where T is the transmission coefficient.

DOI: 10.1002/fld

The boundary conditions on the fictitious interfaces are

$$\phi^{(1)}(-l, y) = \phi^{(2)}(-l, y) \tag{10}$$

$$\left.\frac{\partial \phi^{(1)}}{\partial x}\right|_{x=-l} = \left.\frac{\partial \phi^{(2)}}{\partial x}\right|_{x=-l} \tag{11}$$

$$\phi^{(3)}(l, y) = \phi^{(2)}(l, y) \tag{12}$$

$$\left.\frac{\partial \phi^{(3)}}{\partial x}\right|_{x=l} = \left.\frac{\partial \phi^{(2)}}{\partial x}\right|_{x=l} \tag{13}$$

According to Equations (8)–(10) and (12), we can derive the reflection and transmission coefficients as follows:

$$R = -1 + \frac{k}{n_0 \sinh(kh)} \int_{-h}^{0} \phi^{(2)}(-l, y) \cosh(k(h+y))\, \mathrm{d}y \tag{14}$$

$$T = \frac{k}{n_0 \sinh(kh)} \int_{-h}^{0} \phi^{(2)}(l, y) \cosh(k(h+y))\, \mathrm{d}y \tag{15}$$

where $n_0 = \frac{1}{2}(1 + 2kh/\sinh(2kh))$.

2.2. *Dual boundary integral formulation*

The first equation (*UT* formulation) of the dual boundary integral equations for the domain point can be derived from Green's third identity [18]:

$$2\pi\phi(\tilde{x}) = \int_B T(\tilde{s}, \tilde{x})\phi(\tilde{s})\, \mathrm{d}B(\tilde{s}) - \int_B U(\tilde{s}, \tilde{x}) \frac{\partial \phi(\tilde{s})}{\partial n_{\tilde{s}}}\, \mathrm{d}B(\tilde{s}), \quad \tilde{x} \in D \tag{16}$$

where $\tilde{x}$ is the field point ($\tilde{x} = (x, y)$), $\tilde{s}$ is the source point,

$$U(\tilde{s}, \tilde{x}) = -\mathrm{i} D_0^{(1)}(k|\tilde{s} - \tilde{x}|) \tag{17}$$

in which $D_0^{(1)}(k|\tilde{s} - \tilde{x}|)$ is the first kind of zeroth-order modified Hankel function, and $T(\tilde{s}, \tilde{x})$ is defined by

$$T(\tilde{s}, \tilde{x}) \equiv \frac{\partial U(\tilde{s}, \tilde{x})}{\partial n_{\tilde{s}}} \tag{18}$$

in which $n_{\tilde{s}}$ denotes the normal vector at the boundary point $\tilde{s}$, and $U(\tilde{s}, \tilde{x})$ is the fundamental solution that satisfies

$$\nabla^2 U(\tilde{x}, \tilde{s}) - \lambda^2 U(\tilde{x}, \tilde{s}) = \delta(\tilde{x} - \tilde{s}), \quad \tilde{x} \in D \tag{19}$$

In Equation (19), $\delta(\tilde{x} - \tilde{s})$ is the Dirac-delta function. After taking the normal derivative with respect to Equation (16) for a thin barrier problem, the second equation (*LM* formulation) of the

DOI: 10.1002/fld

dual boundary integral equations for the domain point is derived as

$$2\pi\frac{\partial\phi(\tilde{x})}{\partial n_{\tilde{x}}}=\int_B M(\tilde{s},\tilde{x})\phi(\tilde{s})\,\mathrm{d}B(\tilde{s})-\int_B L(\tilde{s},\tilde{x})\frac{\partial\phi(\tilde{s})}{\partial n_{\tilde{s}}}\,\mathrm{d}B(\tilde{s}),\quad \tilde{x}\in D \tag{20}$$

where

$$L(\tilde{s},\tilde{x})\equiv\frac{\partial U(\tilde{s},\tilde{x})}{\partial n_{\tilde{x}}} \tag{21}$$

$$M(\tilde{s},\tilde{x})\equiv\frac{\partial^2 U(\tilde{s},\tilde{x})}{\partial n_{\tilde{x}}\partial n_{\tilde{s}}} \tag{22}$$

in which $n_{\tilde{x}}$ represents the normal vector of $\tilde{x}$. The explicit forms for the four kernel functions are shown in Table I. By moving the field point $\tilde{x}$ in Equations (16) and (20) to the smooth boundary, the dual boundary integral equations for the boundary point can be obtained as follows:

$$\pi\phi(\tilde{x})=\mathrm{CPV}\int_B T(\tilde{s},\tilde{x})\phi(\tilde{s})\,\mathrm{d}B(\tilde{s})-\mathrm{RPV}\int_B U(\tilde{s},\tilde{x})\frac{\partial\phi(\tilde{s})}{\partial n_{\tilde{s}}}\,\mathrm{d}B(\tilde{s}),\quad \tilde{x}\in B \tag{23}$$

$$\pi\frac{\partial\phi(\tilde{x})}{\partial n_{\tilde{x}}}=\mathrm{HPV}\int_B M(\tilde{s},\tilde{x})\phi(\tilde{s})\,\mathrm{d}B(\tilde{s})-\mathrm{CPV}\int_B L(\tilde{s},\tilde{x})\frac{\partial\phi(\tilde{s})}{\partial n_{\tilde{s}}}\,\mathrm{d}B(\tilde{s}),\quad \tilde{x}\in B \tag{24}$$

where RPV, CPV and HPV are the Riemann, Cauchy and Hadamard (Mangler) principal values, respectively [38].

It must be noted that Equation (24) can be derived simply by applying a normal derivative operator with respect to Equation (23). Differentiation of the Cauchy principal value should be carried out carefully by using Leibnitz's rule. The commutative property provides us with two alternatives for calculating the Hadamard principal value [1]. The four kernel functions, $U(\tilde{s},\tilde{x})$, $T(\tilde{s},\tilde{x})$, $L(\tilde{s},\tilde{x})$ and $M(\tilde{s},\tilde{x})$, in the dual integral equations have different orders of singularity when $\tilde{x}$ approaches $\tilde{s}$. The order of singularity and the symmetry properties for the four kernel functions and the continuous properties of the potentials across the boundary resulting from the four kernel functions are summarized in Table I. The linear algebraic equations discretized from the dual boundary integral equations in Equations (23) and (24) can be expressed as

$$[T]\{\phi\}=[U]\left\{\frac{\partial\phi}{\partial n}\right\} \tag{25}$$

$$[M]\{\phi\}=[L]\left\{\frac{\partial\phi}{\partial n}\right\} \tag{26}$$

where $\{\phi\}$ and $\{\partial\phi/\partial n\}$ are the boundary potential and flux.

After combining the dual equations on the degenerate boundary, when $\tilde{x}$ collocates on degenerate boundaries C^+ or C^-, the singular system of the four influence matrices is desingularized. As either one of the two equations, *UT* or *LM*, for the normal boundary S can be selected, two alternative approaches, $UT+LM$ and $LM+UT$, are proposed.

DOI: 10.1002/fld

Table I. The properties and explicit forms of the kernel functions for the modified Helmholtz equation.

Kernel function $K(\tilde{s},\tilde{x})$	$U(\tilde{s},\tilde{x})$	$T(\tilde{s},\tilde{x})$	$L(\tilde{s},\tilde{x})$	$M(\tilde{s},\tilde{x})$
Explicit forms	$U(\mathbf{s},\mathbf{x})=\mathrm{i}D_0^{(1)}(\lambda r)$	$T(\mathbf{s},\mathbf{x})=-\mathrm{i}\lambda D_1^{(2)}(\lambda r)\frac{y_i n_i}{r}$	$L(\mathbf{s},\mathbf{x})=\mathrm{i}\lambda D_1^{(2)}(\lambda r)\frac{y_i \bar{n}_i}{r}$	$M(\mathbf{s},\mathbf{x})=-\mathrm{i}\lambda\left\{\lambda\frac{D_2^{(1)}(\lambda r)}{r^2}y_i y_j n_i \bar{n}_j+\frac{D_1^{(2)}(\lambda r)}{r}n_i \bar{n}_i\right\}$
Order of singularity	$O(\ln r)$ Weak	$O(1/r)$ Strong	$O(1/r)$ Strong	$O(1/r^2)$ Hypersingular
Symmetry	$U(\tilde{x},\tilde{s})$	$L(\tilde{x},\tilde{s})$	$T(\tilde{x},\tilde{s})$	$M(\tilde{x},\tilde{s})$
Density function $\upsilon(\tilde{s})$	$\frac{\partial\phi}{\partial n}$	ϕ	$\frac{\partial\phi}{\partial n}$	ϕ
Potential type	Single layer	Double layer	Normal derivative of single layer	Normal derivative of double layer
$\int K(\tilde{s},\tilde{x})\upsilon(\tilde{s})\,\mathrm{d}B(\tilde{s})$ continuity across boundary	Continuous	Discontinuous	Discontinuous	Psuedo-continuous
Jump value	No jump	$2\pi\phi$	$2\pi\frac{\partial\phi}{\partial n}$	No jump
Principal value	Riemann	Cauchy	Cauchy	Hadamard

Note: $D_n^{(1)}(\lambda r)=I_n(\lambda r)+\mathrm{i}K_n(\lambda r)$ is the nth-order modified Hankel function of the first kind, $\bar{n}_i$ denotes the ith component of normal vectors on $\tilde{x}$.

DOI: 10.1002/fld

The $UT+LM$ method employs the following equation:

$$\begin{bmatrix} T_{i_S j_S} & T_{i_S j_{C^+}} & T_{i_S j_{C^-}} \\ T_{i_{C^+} j_S} & T_{i_{C^+} j_{C^+}} & T_{i_{C^+} j_{C^-}} \\ M_{i_{C^+} j_S} & M_{i_{C^+} j_{C^+}} & M_{i_{C^+} j_{C^-}} \end{bmatrix} \begin{Bmatrix} \phi_{j_S} \\ \phi_{j_{C^+}} \\ \phi_{j_{C^-}} \end{Bmatrix} = \begin{bmatrix} U_{i_S j_S} & U_{i_S j_{C^+}} & U_{i_S j_{C^-}} \\ U_{i_{C^+} j_S} & U_{i_{C^+} j_{C^+}} & U_{i_{C^+} j_{C^-}} \\ L_{i_{C^+} j_S} & L_{i_{C^+} j_{C^+}} & L_{i_{C^+} j_{C^-}} \end{bmatrix} \begin{Bmatrix} \dfrac{\partial \phi}{\partial n}_{j_S} \\ \dfrac{\partial \phi}{\partial n}_{j_{C^+}} \\ \dfrac{\partial \phi}{\partial n}_{j_{C^-}} \end{Bmatrix} \tag{27}$$

where i_S and i_{C^+} denote the collocation points on the S and C^+ boundaries, respectively, and j_S and j_{C^+} denote the element ID on the S and C^+ boundaries, respectively. Also, $LM+UT$ method can solve the degenerate boundary problem by using

$$\begin{bmatrix} M_{i_S j_S} & M_{i_S j_{C^+}} & M_{i_S j_{C^-}} \\ T_{i_{C^+} j_S} & T_{i_{C^+} j_{C^+}} & T_{i_{C^+} j_{C^-}} \\ M_{i_{C^+} j_S} & M_{i_{C^+} j_{C^+}} & M_{i_{C^+} j_{C^-}} \end{bmatrix} \begin{Bmatrix} \phi_{j_S} \\ \phi_{j_{C^+}} \\ \phi_{j_{C^-}} \end{Bmatrix} = \begin{bmatrix} L_{i_S j_S} & L_{i_S j_{C^+}} & L_{i_S j_{C^-}} \\ U_{i_{C^+} j_S} & U_{i_{C^+} j_{C^+}} & U_{i_{C^+} j_{C^-}} \\ L_{i_{C^+} j_S} & L_{i_{C^+} j_{C^+}} & L_{i_{C^+} j_{C^-}} \end{bmatrix} \begin{Bmatrix} \dfrac{\partial \phi}{\partial n}_{j_S} \\ \dfrac{\partial \phi}{\partial n}_{j_{C^+}} \\ \dfrac{\partial \phi}{\partial n}_{j_{C^-}} \end{Bmatrix} \tag{28}$$

The main difference between Equations (27) and (28) is the constraint obtained by collocating the points on the normal boundary (S), using the UT and LM equations, respectively.

2.3. Expanding the four kernels using the multipole expansion method

By adopting the addition theorem, the four kernels in the dual formulation are expanded into degenerate kernels that separate the field point and the source point. The kernel function, $U(\tilde{s}, \tilde{x})$, can be expanded into

$$\begin{aligned} U(\tilde{s}, \tilde{x}) &= \sum_{m=0}^{\infty} C_m(\tilde{x}) R_m(\tilde{s}) \\ &= \begin{cases} U^i = \sqrt{-1} \sum_{m=0}^{\infty} \varepsilon_m (-1)^m I_m(k|\tilde{x}-\tilde{p}|) F_m(k|\tilde{s}-\tilde{p}|) \cos(m\alpha) \\ \qquad |\tilde{s}-\tilde{p}| > |\tilde{x}-\tilde{p}| \\ U^e = \sqrt{-1} \sum_{m=0}^{\infty} \varepsilon_m (-1)^m F_m(k|\tilde{x}-\tilde{p}|) I_m(k|\tilde{s}-\tilde{p}|) \cos(m\alpha) \\ \qquad |\tilde{x}-\tilde{p}| > |\tilde{s}-\tilde{p}| \end{cases} \end{aligned} \tag{29}$$

DOI: 10.1002/fld

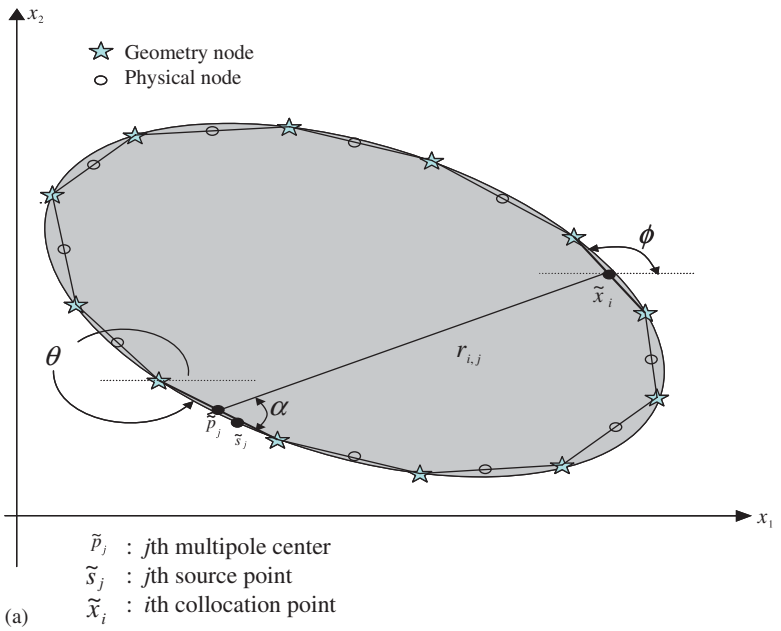

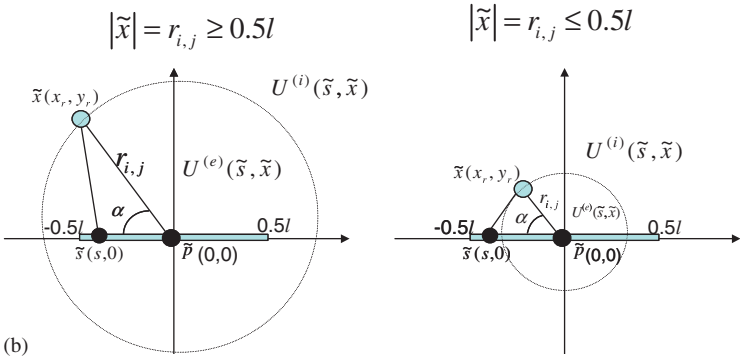

Figure 2. The definition sketch of the coordinate and coordinate transformation of collocation point: (a) global coordinate; (b) local coordinate; and (c) coordinate transformation of collocation point.

DOI: 10.1002/fld

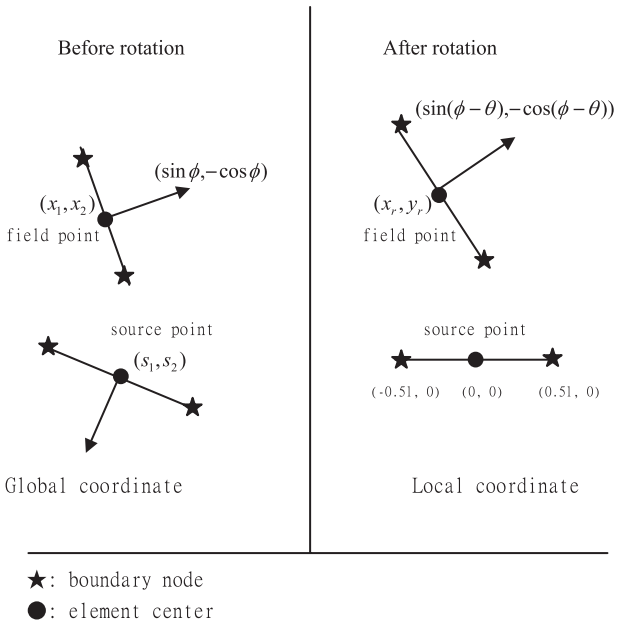

(c)
$$\begin{Bmatrix} x_r \\ y_r \end{Bmatrix} = \begin{bmatrix} \cos\theta & \sin\theta \\ -\sin\theta & \cos\theta \end{bmatrix} \begin{Bmatrix} x_1 - s_1 \\ x_2 - s_2 \end{Bmatrix}$$

Figure 2. *Continued.*

where $C_m(\tilde{x})$ and $R_m(\tilde{x})$ are the field point function and the source point function of U kernel, respectively, $\tilde{p}$ is the center of the multipole and

$$\varepsilon_m = \begin{Bmatrix} 1, & m=0 \\ 2, & m\neq 0 \end{Bmatrix} \tag{30}$$

$$\alpha = \cos^{-1}\left(\frac{(\tilde{s}-\tilde{p})\cdot(\tilde{x}-\tilde{p})}{|\tilde{s}-\tilde{p}||\tilde{x}-\tilde{p}|}\right) \tag{31}$$

and

$$F_m = I_m + \sqrt{-1}(-1)^m K_m \tag{32}$$

in which I_m and K_m are the mth-order modified Bessel functions of the first kind and second kind, respectively. The definition sketch of the global coordinate is shown in Figure 2(a). The contour plot of potential for the U kernel can be shown in Figures 3(a) and (b) for the real part and imaginary part of the series form using the degenerate kernel in Equation (29), and Figures 3(c) and (d) for the real part and imaginary part of the closed-form solution using Equation (17). The

DOI: 10.1002/fld

kernel function, $T(\tilde{s},\tilde{x})$, can be expanded into

$$T(\tilde{s},\tilde{x})=\sum_{m=0}^{\infty}C_m(\tilde{x})[\nabla R_m(\tilde{s})\cdot n_s]$$

$$=\begin{cases} T^i=\sqrt{-1}\displaystyle\sum_{m=0}^{\infty}\varepsilon_m(-1)^m I_m(k|\tilde{x}-\tilde{p}|) \\ \qquad\times\left\{\dfrac{\partial F_m(k|\tilde{s}-\tilde{p}|)}{\partial n_s}\cos(m\alpha)+F_m(k|\tilde{s}-\tilde{p}|)\dfrac{\partial\cos(m\alpha)}{\partial n_s}\right\} \\ \qquad|\tilde{s}-\tilde{p}|>|\tilde{x}-\tilde{p}| \\ T^e=\sqrt{-1}\displaystyle\sum_{m=0}^{\infty}\varepsilon_m(-1)^m F_m(k|\tilde{x}-\tilde{p}|) \\ \qquad\times\left\{\dfrac{\partial I_m(k|\tilde{s}-\tilde{p}|)}{\partial n_s}\cos(m\alpha)+I_m(k|\tilde{s}-\tilde{p}|)\dfrac{\partial\cos(m\alpha)}{\partial n_s}\right\} \\ \qquad|\tilde{x}-\tilde{p}|>|\tilde{s}-\tilde{p}| \end{cases} \tag{33}$$

where

$$\frac{\partial I_m(k|\tilde{s}-\tilde{p}|)}{\partial n_s}=\frac{k}{2}[I_{m-1}(k|\tilde{s}-\tilde{p}|)+I_{m+1}(k|\tilde{s}-\tilde{p}|)]\frac{(s_i-p_i)n_i}{|\tilde{s}-\tilde{p}|} \tag{34}$$

$$\frac{\partial F_m(k|\tilde{s}-\tilde{p}|)}{\partial n_s}=\frac{k}{2}[F_{m-1}(k|\tilde{s}-\tilde{p}|)+F_{m+1}(k|\tilde{s}-\tilde{p}|)]\frac{(s_i-p_i)n_i}{|\tilde{s}-\tilde{p}|} \tag{35}$$

$$\frac{\partial\cos(m\alpha)}{\partial n_s}=-m\sin(m\alpha)(a_i n_i) \tag{36}$$

in which n_i is the ith component of the normal vector at $\tilde{s}$ and

$$a_1=\frac{-1}{\sin(\alpha)}\frac{(s_2-p_2)^2(x_1-p_1)-(s_1-p_1)(s_2-p_2)(x_2-p_2)}{|\tilde{s}-\tilde{p}|^3|\tilde{x}-\tilde{p}|} \tag{37}$$

$$a_2=\frac{-1}{\sin(\alpha)}\frac{(s_1-p_1)^2(x_2-p_2)-(s_1-p_1)(s_2-p_2)(x_1-p_1)}{|\tilde{s}-\tilde{p}|^3|\tilde{x}-\tilde{p}|} \tag{38}$$

DOI: 10.1002/fld

The kernel function, $L(\tilde{s},\tilde{x})$, can be expanded into

$$L(\tilde{s},\tilde{x})=\sum_{m=0}^{\infty}[\nabla C_m(\tilde{x})\cdot n_x]R_m(\tilde{s})$$

$$=\begin{cases} L^i=\sqrt{-1}\displaystyle\sum_{m=0}^{\infty}\varepsilon_m(-1)^m F_m(k|\tilde{s}-\tilde{p}|) \\ \qquad\times\left\{\dfrac{\partial I_m(k|\tilde{x}-\tilde{p}|)}{\partial n_x}\cos(m\alpha)+I_m(k|\tilde{x}-\tilde{p}|)\dfrac{\partial\cos(m\alpha)}{\partial n_x}\right\} \\ \qquad|\tilde{s}-\tilde{p}|>|\tilde{x}-\tilde{p}| \\ L^e=\sqrt{-1}\displaystyle\sum_{m=0}^{\infty}\varepsilon_m(-1)^m I_m(k|\tilde{s}-\tilde{p}|) \\ \qquad\times\left\{\dfrac{\partial F_m(k|\tilde{x}-\tilde{p}|)}{\partial n_x}\cos(m\alpha)+F_m(k|\tilde{x}-\tilde{p}|)\dfrac{\partial\cos(m\alpha)}{\partial n_x}\right\} \\ \qquad|\tilde{x}-\tilde{p}|>|\tilde{s}-\tilde{p}| \end{cases} \tag{39}$$

where

$$\frac{\partial I_m(k|\tilde{x}-\tilde{p}|)}{\partial n_x}=\frac{k}{2}[I_{m-1}(k|\tilde{x}-\tilde{p}|)+I_{m+1}(k|\tilde{x}-\tilde{p}|)]\frac{(x_i-p_i)\bar{n}_i}{|\tilde{x}-\tilde{p}|} \tag{40}$$

$$\frac{\partial F_m(k|\tilde{x}-\tilde{p}|)}{\partial n_x}=\frac{k}{2}[F_{m-1}(k|\tilde{x}-\tilde{p}|)+F_{m+1}(k|\tilde{x}-\tilde{p}|)]\frac{(x_i-p_i)\bar{n}_i}{|\tilde{x}-\tilde{p}|} \tag{41}$$

$$\frac{\partial\cos(m\alpha)}{\partial n_x}=-m\sin(m\alpha)(b_i\bar{n}_i) \tag{42}$$

in which $\bar{n}_i$ is the ith component of the normal vector at $\tilde{x}$ and

$$b_1=\frac{-1}{\sin(\alpha)}\frac{(s_1-p_1)(x_2-p_2)^2-(s_2-p_2)(x_1-p_1)(x_2-p_2)}{|\tilde{x}-\tilde{p}|^3|\tilde{s}-\tilde{p}|} \tag{43}$$

$$b_2=\frac{-1}{\sin(\alpha)}\frac{(s_2-p_2)(x_1-p_1)^2-(s_1-p_1)(x_1-p_1)(x_2-p_2)}{|\tilde{x}-\tilde{p}|^3|\tilde{s}-\tilde{p}|} \tag{44}$$

DOI: 10.1002/fld

The kernel function, $M(\tilde{s},\tilde{x})$, can be expanded into

$$
\begin{aligned}
M(\tilde{s},\tilde{x}) &= \sum_{m=0}^{\infty} [\nabla C_m(\tilde{x})\cdot n_x][\nabla R_m(\tilde{s})\cdot n_s] \\
&= \begin{cases}
M^i = \sqrt{-1}\sum\limits_{m=0}^{\infty} \varepsilon_m(-1)^m \\
\quad \times \left\{ \dfrac{\partial F_m(k|\tilde{s}-\tilde{p}|)}{\partial n_s}\left[\dfrac{\partial I_m(k|\tilde{x}-\tilde{p}|)}{\partial n_x}\cos(m\alpha) + I_m(k|\tilde{x}-\tilde{p}|)\dfrac{\partial \cos(m\alpha)}{\partial n_x}\right]\right. \\
\quad \left. + F_m(k|\tilde{s}-\tilde{p}|)\left[\dfrac{\partial I_m(k|\tilde{x}-\tilde{p}|)}{\partial n_x}\dfrac{\partial \cos(m\alpha)}{\partial n_s} + I_m(k|\tilde{x}-\tilde{p}|)\dfrac{\partial^2 \cos(m\alpha)}{\partial n_x \partial n_s}\right]\right\} \\
\quad |\tilde{s}-\tilde{p}| > |\tilde{x}-\tilde{p}| \\
M^e = \sqrt{-1}\sum\limits_{m=0}^{\infty} \varepsilon_m(-1)^m \\
\quad \times \left\{ \dfrac{\partial I_m(k|\tilde{s}-\tilde{p}|)}{\partial n_s}\left[\dfrac{\partial F_m(k|\tilde{x}-\tilde{p}|)}{\partial n_x}\cos(m\alpha) + F_m(k|\tilde{x}-\tilde{p}|)\dfrac{\partial \cos(m\alpha)}{\partial n_x}\right]\right. \\
\quad \left. + I_m(k|\tilde{s}-\tilde{p}|)\left[\dfrac{\partial F_m(k|\tilde{x}-\tilde{p}|)}{\partial n_x}\dfrac{\partial \cos(m\alpha)}{\partial n_s} + F_m(k|\tilde{x}-\tilde{p}|)\dfrac{\partial^2 \cos(m\alpha)}{\partial n_x \partial n_s}\right]\right\} \\
\quad |\tilde{x}-\tilde{p}| > |\tilde{s}-\tilde{p}|
\end{cases}
\end{aligned} \tag{45}
$$

where

$$
\begin{aligned}
\frac{\partial^2 \cos(m\alpha)}{\partial n_x \partial n_s} &= \frac{\partial[-m\sin(m\alpha)a_i n_i]}{\partial n_x} \\
&= a_i n_i \frac{\partial[-m\sin(m\alpha)]}{\partial n_x} + (-m\sin(m\alpha))\frac{\partial a_i n_i}{\partial n_x} \\
&= a_i n_i[-m^2\cos(m\alpha)b_i\bar{n}_i] \\
&\quad +[-m\sin(m\alpha)]\left\{ n_1\left[\frac{-(s_2-p_2)}{|\tilde{s}-\tilde{p}|^3}\left(\frac{\bar{n}_1}{x_2-p_2} - \frac{(x_1-p_1)\bar{n}_1}{(x_2-p_2)^2}\right)\right]\right. \\
&\quad \left. + n_2\left[\frac{(s_1-p_1)(s_2-p_2)}{|\tilde{s}-\tilde{p}|^3}\left(\frac{\bar{n}_1}{x_2-p_2} - \frac{(x_1-p_1)\bar{n}_1}{(x_2-p_2)^2}\right)\right]\right\}
\end{aligned} \tag{46}
$$

2.4. Dual boundary element formulation in conjunction with the FMM

By employing the constant element scheme through coordinate transformation and moving the center of the multipole, $\tilde{p}$, to the center of the local coordinate on each boundary element as shown

DOI: 10.1002/fld

in Figure 2(b), each element of the influence matrices can be obtained as follows:

(1) U kernel: For the regular integral ($i \neq j$), we have

(a) $r_{ij} > 0.5l_j$

$$U_{ij} = \int_{-0.5l_j}^{0.5l_j} U^e \, \mathrm{d}s$$

$$= 4\sqrt{-1} \sum_{m=0}^{\infty} \varepsilon_m F_{2m}(kr_{ij}) \cos(2m\alpha) \int_{-0.5l_j}^{0.5l_j} I_{2m}(k|s|) \, \mathrm{d}s$$

$$= \sum_{m=0}^{\infty} C^1_{ijm} R_{mj} \tag{47}$$

where r_{ij} is the distance between the collocation point on the center of the ith element and the source point on the center of the jth element, $r_{ij} = \sqrt{x_r^2 + y_r^2}$, x_r and y_r are the coordinates of the collocation point after translation and rotation as shown in Figure 2(c) and l_j is the length of the jth source element. The multipole moment R_{mj} is the value related to the source point coordinate and C^1_{ijm} is the value related to the field point coordinate as shown below:

$$C^1_{ijm} = 4\sqrt{-1}\varepsilon_m F_{2m}(kr_{ij}) \cos(2m\alpha) \tag{48}$$

$$R_{mj} = \frac{1}{k} \sum_{n=0}^{\infty} (-1)^n I_{2m+2n+1}(0.5l_j) \tag{49}$$

(b) $r_{ij} < 0.5l_j$

$$U_{ij} = \int_{-0.5l_j}^{-r_{ij}} U^i \, \mathrm{d}s + \int_{-r_{ij}}^{r_{ij}} U^e \, \mathrm{d}s + \int_{r_{ij}}^{0.5l_j} U^i \, \mathrm{d}s$$

$$= 4\sqrt{-1} \sum_{m=0}^{\infty} \varepsilon_m F_{2m}(kr_{ij}) \cos(2m\alpha) \left(\frac{1}{k} \sum_{n=0}^{n=\infty} (-1)^n I_{2m+2n+1}(kr_{ij}) \right)$$

$$+ 4\sqrt{-1} \sum_{m=0}^{\infty} \varepsilon_m (-1)^m I_{2m}(kr_{ij}) \cos(2m\alpha) \int_{r_{ij}}^{0.5l_j} F_{2m}(k|s|) \, \mathrm{d}s \tag{50}$$

For the weakly singular integral ($i = j$), we regularize the integral by means of partial integration and limiting process ($(x_r, y_r) = (0, \varepsilon)$) as follows:

$$U_{ii} = \lim_{\varepsilon \to 0} \int_{-0.5l_j}^{-\varepsilon} U^i \, \mathrm{d}s + \int_{-\varepsilon}^{\varepsilon} U^e \, \mathrm{d}s + \int_{\varepsilon}^{0.5l_j} U^i \, \mathrm{d}s \quad (i \text{ no sum})$$

$$= 2\sqrt{-1} \sum_{m=0}^{\infty} \varepsilon_m (-1)^m F_{2m}(k\varepsilon) \cos(m\pi) \left\{ \frac{1}{k} \sum_{n=0}^{n=\infty} (-1)^n I_{2m+2n+1}(k\varepsilon) \right.$$

DOI: 10.1002/fld

$$+2\sqrt{-1}\sum_{m=0}^{\infty}\varepsilon_m I_{2m}(k\varepsilon)\cos(m\pi)\left(\int_{\varepsilon}^{0.5l_j}F_m(k|s|)\,\mathrm{d}s\right)\Bigg\}$$

$$=\sqrt{-1}\left\{D_0^{(1)}\left(\frac{kl}{2}\right)l-k\int_{-0.5l_j}^{0.5l_j}\{D_1^{(2)}(k|s|)|s|\,\mathrm{d}s\}\right\} \tag{51}$$

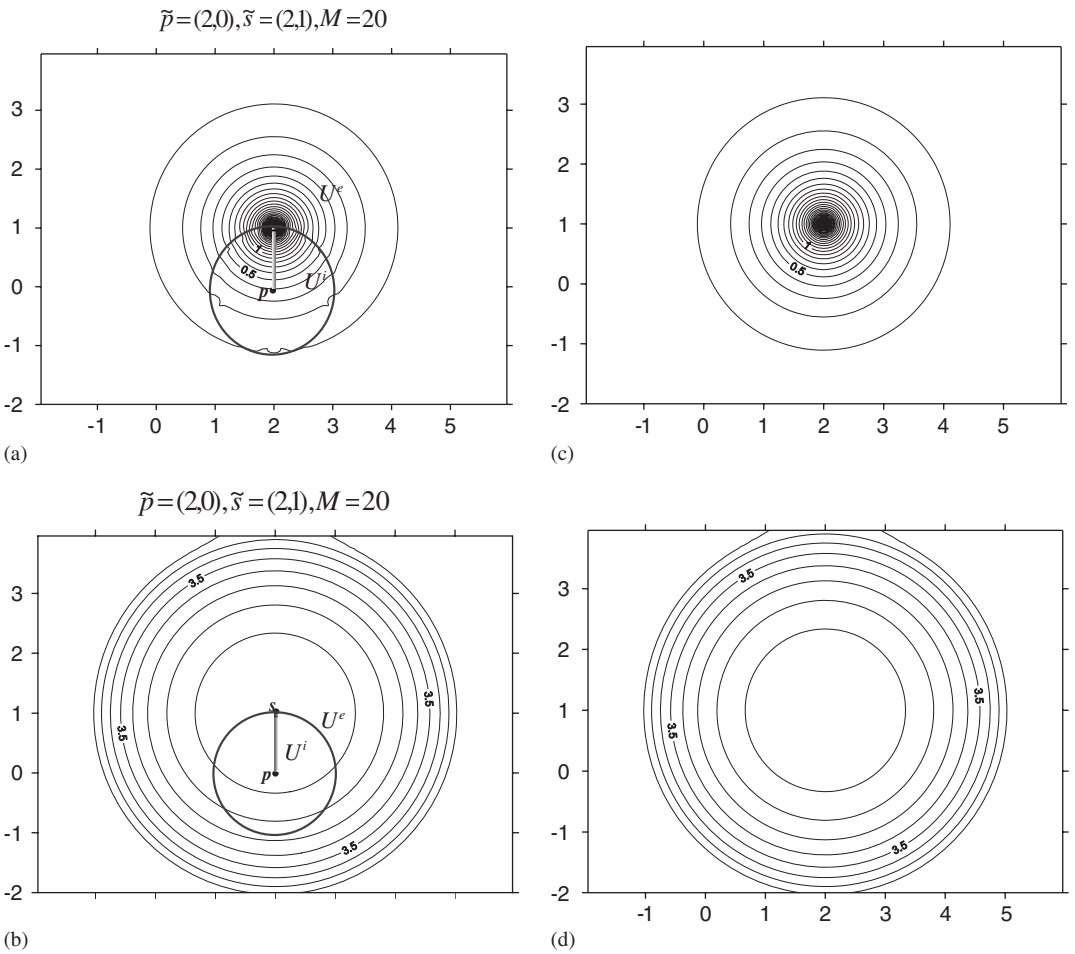

Figure 3. The contour plot of potential for U kernel: (a) the real part of U kernel using degenerate form of Equation (29); (b) the imaginary part of U kernel using degenerate form of Equation (29); (c) the real part of U kernel using the closed-form solution of Equation (17); and (d) the imaginary part of U kernel using the closed-form solution of Equation (17).

DOI: 10.1002/fld

where

$$\lim_{\varepsilon\to 0}\int_{-\varepsilon}^{\varepsilon} F_0^{(1)}(k|s|)\,\mathrm{d}s=\lim_{\varepsilon\to 0}\int_{-\varepsilon}^{\varepsilon}-\sqrt{-1}\ln(k|s|)\,\mathrm{d}s=0 \tag{52}$$

(2) T kernel: For the regular integral ($i\neq j$), we have
(a) $r_{ij}>0.5l$

$$\begin{aligned}T_{ij}&=\int_{-0.5l_j}^{0.5l_j} T^e\,\mathrm{d}s\\&=\sqrt{-1}\sum_{m=0}^{\infty}\varepsilon_m(-1)_{2m}F_{2m}(kr_{ij})\cos(2m\alpha)\\&\quad\times\int_{-0.5l_j}^{0.5l_j}\frac{k}{2}[I_{2m-1}(k|s|)+I_{2m+1}(k|s|)]\frac{s\cdot 0+0\cdot(-1)}{|s|}\,\mathrm{d}s\\&\quad+\sqrt{-1}\sum_{m=0}^{\infty}2F_{2m+1}(kr_{ij})(2m+1)\sin((2m+1)\alpha)\int_{-0.5l_j}^{0.5l_j}\frac{I_{2m+1}(k|s|)}{|s|}\,\mathrm{d}s\\&=C_{ijm}^2[R_{mj}-R_{(m+1)j}]\end{aligned} \tag{53}$$

where

$$C_{ijm}^2=4\sqrt{-1}kF_{2m+1}(kr_{ij})\sin((2m+1)\alpha) \tag{54}$$

(b) $r_{ij}<0.5l$

$$\begin{aligned}T_{ij}&=\int_{-0.5l_j}^{-r_{ij}}T^i\,\mathrm{d}s+\int_{-r_{ij}}^{r_{ij}}T^e\,\mathrm{d}s+\int_{r_{ij}}^{0.5l_j}T^i\,\mathrm{d}s\\&=4\sqrt{-1}\sum_{m=0}^{\infty}F_{2m+1}(kr_{ij})\sin((2m+1)\alpha)\\&\quad\times\sum_{n=0}^{\infty}(-1)^n[I_{2m+2n+1}(kr_{ij})-I_{2m+2n+3}(kr_{ij})]\\&\quad+4\sqrt{-1}\sum_{m=0}^{\infty}I_{2m+1}(kr_{ij})(2m+1)\sin((2m+1)\alpha)\frac{k}{4m+2}\\&\quad\times\int_{r_{ij}}^{0.5l_j}[F_{2m}(k|s|)-F_{2m+2}(k|s|)]\,\mathrm{d}s\end{aligned} \tag{55}$$

For the strongly singular integral ($i=j$), we regularize the integral by means of partial integration, limiting process and the identity from the generalized function [39] as shown below:

$$\sum_{m=1}^{\infty}\frac{\sin(m\pi/2)}{m}=\frac{\pi}{4} \tag{56}$$

DOI: 10.1002/fld

We can obtain the integral as follows:

$$
\begin{aligned}
T_{ii} &= \int_{-0.5l_j}^{-\varepsilon} T^i \,\mathrm{d}s + \int_{-\varepsilon}^{\varepsilon} T^e \,\mathrm{d}s + \int_{\varepsilon}^{0.5l_j} T^i \,\mathrm{d}s \quad (i \text{ no sum}) \\
&= 4\sqrt{-1} \sum_{m=0}^{\infty} F_{2m+1}(k\varepsilon) \sin((2m+1)\alpha) \sum_{n=0}^{\infty} (-1)^n [I_{2m+2n+1}(k\varepsilon) - I_{2m+2n+3}(k\varepsilon)] \\
&\quad + 4\sqrt{-1} \sum_{m=0}^{\infty} I_{2m+1}(kr_{ij})(2m+1) \sin((2m+1)\alpha) \frac{k}{4m+2} \int_{\varepsilon}^{0.5l_j} [F_{2m}(k|s|) - F_{2m+2}(k|s|)] \,\mathrm{d}s \\
&= 2 \sum_{m=1}^{\infty} \frac{\sin(m\pi/2)}{m} + 2 \sum_{m=1}^{\infty} \frac{\sin(m\pi/2)}{m} \\
&= \pi
\end{aligned} \tag{57}
$$

(3) L kernel: For the regular integral ($i \neq j$), we have
(a) $r_{ij} > 0.5l$

$$
\begin{aligned}
L_{ij} &= \int_{-0.5l_j}^{0.5l_j} L^e \,\mathrm{d}s \\
&= \sqrt{-1} \sum_{m=0}^{\infty} \varepsilon_m (-1)^{2m} \frac{k}{2} [F_{2m-1}^{(1)}(kr_{ij}) + F_{2m+1}(kr_{ij})] \frac{x_i \bar{n}_i}{r_{ij}} \cos(2m\alpha) \int_{-0.5l_j}^{0.5l_j} I_{2m}(k|s|) \,\mathrm{d}s \\
&\quad - \sqrt{-1} \sum_{m=0}^{\infty} \varepsilon_m (-1)^{2m} F_{2m}(kr_{ij})(2m) \sin(2m\alpha) \frac{y_r \bar{n}_1 - x_r \bar{n}_2}{r_{ij}^2} \int_{-0.5l_j}^{0.5l_j} I_{2m}(k|s|) \,\mathrm{d}s \\
&= \sum_{m=0}^{\infty} C_{ijm}^3 R_{mj}
\end{aligned} \tag{58}
$$

where

$$
\begin{aligned}
C_{ijm}^3 = \sqrt{-1}\varepsilon_m \Bigg\{ & \frac{k}{2} [F_{2m-1}(kr_{ij}) - F_{2m+1}(kr_{ij})] \frac{x_i \bar{n}_i}{r_{ij}} \cos(2m\alpha) \\
& - F_{2m}(kr_{ij})(2m) \sin(2m\alpha) \frac{y_r \bar{n}_1 - x_r \bar{n}_2}{r_{ij}^2} \Bigg\}
\end{aligned} \tag{59}
$$

(b) $r_{ij} < 0.5l$

$$
\begin{aligned}
L_{ij} &= \int_{-0.5l_j}^{-r_{ij}} L^i \,\mathrm{d}s + \int_{-r_{ij}}^{r_{ij}} L^e \,\mathrm{d}s + \int_{r_{ij}}^{0.5l_j} L^i \,\mathrm{d}s \\
&= \sqrt{-1} \sum_{m=0}^{\infty} \varepsilon_m (-1)^{2m} \frac{k}{2} [F_{2m-1}(kr_{ij}) + F_{2m+1}(kr_{ij})] \frac{x_i \bar{n}_i}{r_{ij}}
\end{aligned}
$$

DOI: 10.1002/fld

$$\times \cos(2m\alpha)\frac{4}{k}\left[\sum_{n=0}^{\infty}(-1)^n I_{2m+2n+1}(kr_{ij})\right]$$

$$+\sqrt{-1}\sum_{m=0}^{\infty}\varepsilon_m F_{2m}(kr_{ij})(2m)\sin(2m\alpha)\frac{y_r\bar{n}_1 - x_r\bar{n}_2}{r_{ij}^2}\frac{4}{k}\left[\sum_{n=0}^{\infty}(-1)^n I_{2m+2n+1}(kr_{ij})\right]$$

$$+2\sqrt{-1}\sum_{m=0}^{\infty}\varepsilon_m\frac{k}{2}[I_{2m-1}(kr_{ij})+I_{2m+1}(kr_{ij})]\frac{x_i\bar{n}_i}{r_{ij}}\cos(2m\alpha)\int_{r_{ij}}^{0.5l_j}F_{2m}(ks)\,\mathrm{d}s$$

$$+2\sqrt{-1}\sum_{m=0}^{\infty}\varepsilon_m I_{2m}(kr_{ij})(2m)\sin(2m\alpha)\frac{y_r\bar{n}_1 - x_r\bar{n}_2}{r_{ij}^2}\int_{r_{ij}}^{0.5l_j}F_{2m}(k|s|)\,\mathrm{d}s \tag{60}$$

For the strongly singular integral ($i = j$), we regularize the integral by means of partial integration and limiting process and the identity in Equation (56) as follows:

$$\begin{aligned}
L_{ii} &= \int_{-0.5l_j}^{-\varepsilon} L^i\,\mathrm{d}s + \int_{-\varepsilon}^{\varepsilon} L^e\,\mathrm{d}s + \int_{\varepsilon}^{0.5l_j} L^i\,\mathrm{d}s \quad (i \text{ no sum})\\
&= \sqrt{-1}\sum_{m=0}^{\infty}\varepsilon_m(-1)^{2m}\frac{k}{2}[F_{2m-1}(k\varepsilon)+F_{2m+1}(k\varepsilon)]\frac{x_i\bar{n}_i}{r_{ij}}\cos(2m\alpha)\frac{4}{k}\left[\sum_{n=0}^{\infty}(-1)^n I_{2m+2n+1}(k\varepsilon)\right]\\
&\quad +2\sqrt{-1}\sum_{m=0}^{\infty}\varepsilon_m\frac{k}{2}[I_{2m-1}(k\varepsilon)+I_{2m+1}(k\varepsilon)](-1)^m\int_{\varepsilon}^{0.5l_j}F_{2m}(k|s|)\,\mathrm{d}s\\
&= -2\left[\sum_{m=1}^{\infty}\frac{\sin(m\pi/2)}{m}-1\right]-2-2\left[\sum_{m=1}^{\infty}\frac{\sin(m\pi/2)}{m}\right]\\
&= -\pi
\end{aligned} \tag{61}$$

(4) M kernel: For the regular integral ($i \neq j$), we have
(a) $r_{ij} > 0.5l$

$$\begin{aligned}
M_{ij} &= \int_{-0.5l_j}^{0.5l_j} M^e\,\mathrm{d}s\\
&= \sqrt{-1}\sum_{m=0}^{\infty}(2)\frac{k}{2}[F_{2m}(kr_{ij})+F_{2m+2}(kr_{ij})]\frac{x_i\bar{n}_i}{r_{ij}}[(2m+1)\sin((2m+1)\alpha)]\\
&\quad\times\int_{-0.5l_j}^{0.5l_j}\frac{I_{2m+1}(k|s|)}{|s|}\,\mathrm{d}s - \sqrt{-1}\sum_{m=0}^{\infty}(2)F_{2m+1}(kr_{ij})(2m+1)^2\cos((2m+1)\alpha)\\
&\quad\times\frac{y_r\bar{n}_1 - x_r\bar{n}_2}{r_{ij}^2}\int_{-0.5l_j}^{0.5l_j}\frac{I_{2m+1}(k|s|)}{|s|}\,\mathrm{d}s\\
&= \sum_{m=0}^{\infty}C_{ijm}^4[R_{mj}+R_{(m+1)j}]
\end{aligned} \tag{62}$$

DOI: 10.1002/fld

where

$$C_{ijm}^4 = \sqrt{-1}k\frac{x_i\bar{n}_i}{r_{ij}}(2m+1)\left\{k[F_{2m}(kr_{ij})+F_{2m+2}(kr_{ij})]\sin((2m+1)\alpha)\right.$$
$$\left.+F_{2m+1}(kr_{ij})(2m+1)\cos((2m+1)\alpha)\frac{y_r\bar{n}_1-x_r\bar{n}_2}{kr_{ij}}\right\} \tag{63}$$

(b) $r_{ij}<0.5l$

$$M_{ij}=\int_{-0.5l_j}^{-r_{ij}}M^i\,\mathrm{d}s+\int_{-r_{ij}}^{r_{ij}}M^e\,\mathrm{d}s+\int_{r_{ij}}^{0.5l_j}M^i\,\mathrm{d}s$$
$$=\sqrt{-1}\sum_{m=0}^{\infty}(2)\frac{k}{2}[F_{2m}(kr_{ij})+F_{2m+2}(kr_{ij})]\frac{x_i\bar{n}_i}{r_{ij}}[(2m+1)\sin((2m+1)\alpha)]$$
$$\times\frac{2}{2m+1}\sum_{n=0}^{\infty}(-1)^n\left[I_{2m+2n+1}\left(\frac{kl}{2}\right)+I_{2m+2n+3}\left(\frac{kl}{2}\right)\right]$$
$$-\sqrt{-1}\sum_{m=0}^{\infty}(2)F_{2m+1}(kr_{ij})(2m+1)^2\cos((2m+1)\alpha)$$
$$\times\frac{y_r\bar{n}_1-x_r\bar{n}_2}{r_{ij}^2}\frac{2}{2m+1}\sum_{n=0}^{\infty}(-1)^n[I_{2m+2n+1}(kr_{ij})+I_{2m+2n+3}(kr_{ij})]$$
$$+\frac{2\sqrt{-1}}{r_{ij}^2}\sum_{m=0}^{\infty}(2m+1)\left\{\frac{k}{2}(r_{ij})[I_{2m}(kr_{ij})+I_{2m+2}(kr_{ij})]x_i\bar{n}_i\sin((2m+1)\alpha)\right.$$
$$\left.+I_{2m+1}(kr_{ij})(2m+1)\cos((2m+1)\alpha)y_r\bar{n}_1-x_r\bar{n}_2\right\}\frac{k}{4m+2}$$
$$\times\int_{r_{ij}}^{0.5l_j}[F_{2m}(k|s|)+F_{2m+2}(k|s|)]\,\mathrm{d}s \tag{64}$$

For the hypersingular integral ($i=j$), we regularize the integral by means of partial integration, limiting process and using the identity from the generalized function [39] as shown below:

$$\sum_{m=0}^{\infty}(-1)^m=\frac{1}{2} \tag{65}$$

We can obtain the integral as follows:

$$M_{ii}=\int_{-0.5l_j}^{-\varepsilon}M^i\,\mathrm{d}s+\int_{-\varepsilon}^{\varepsilon}M^e\,\mathrm{d}s+\int_{\varepsilon}^{0.5l_j}M^i\,\mathrm{d}s\quad(i\text{ no sum})$$
$$=-2\sqrt{-1}k\left\{\int_{\varepsilon}^{0.5l_j}\frac{F_1(k|s|)}{|s|}\,\mathrm{d}s+\sum_{m=1}^{\infty}I_{2m}(k\varepsilon)(2m+1)(-1)^m\int_{\varepsilon}^{0.5l_j}\frac{F_{2m+1}(k|s|)}{|s|}\,\mathrm{d}s\right\}$$

DOI: 10.1002/fld

$$+\sum_{m=1}^{\infty}\frac{2(2m+1)(-1)^m}{\varepsilon^{2m+2}}\int_0^{\varepsilon}s^{2m}\,\mathrm{d}s$$
$$=2\sqrt{-1}kD_1^{(2)}\left(\frac{kl}{2}\right)-k^2U_{ii} \tag{66}$$

It is interesting to find that R_{mj} term is repeatedly embedded in the formulae of the four influence matrices of Equations (47), (53), (58) and (62).

2.5. Construction of the four influence matrices

By using the derivations of Section 2.4 and adopting $M+1$ terms in the series sum, the four influence matrices in Equations (25) and (26) can be rewritten as

$$[U]=\begin{bmatrix}0 & 0 & \cdots & 0\\ C^1_{210} & C^1_{211} & \cdots & C^1_{21M}\\ \vdots & \vdots & \ddots & \vdots\\ C^1_{N10} & C^1_{N11} & \cdots & C^1_{N1M}\end{bmatrix}_{N\times(M+1)}\begin{bmatrix}R_{01} & 0 & \cdots & 0\\ R_{11} & 0 & \cdots & 0\\ \vdots & \vdots & \ddots & \vdots\\ R_{M1} & 0 & \cdots & 0\end{bmatrix}_{(M+1)\times N}$$
$$+\begin{bmatrix}C^1_{120} & C^1_{121} & \cdots & C^1_{12M}\\ 0 & 0 & \cdots & 0\\ \vdots & \vdots & \ddots & \vdots\\ C^1_{N20} & C^1_{N21} & \cdots & C^1_{N2M}\end{bmatrix}_{N\times(M+1)}\begin{bmatrix}0 & R_{02} & \cdots & 0\\ 0 & R_{12} & \cdots & 0\\ \vdots & \vdots & \ddots & \vdots\\ 0 & R_{M2} & \cdots & 0\end{bmatrix}_{(M+1)\times N}$$
$$+\cdots+\begin{bmatrix}C^1_{1N0} & C^1_{1N1} & \cdots & C^1_{1NM}\\ C^1_{2N0} & C^1_{2N1} & \cdots & C^1_{2NM}\\ \vdots & \vdots & \ddots & \vdots\\ 0 & 0 & \cdots & 0\end{bmatrix}_{N\times(M+1)}\begin{bmatrix}0 & 0 & \cdots & R_{0N}\\ 0 & 0 & \cdots & R_{1N}\\ \vdots & \vdots & \ddots & \vdots\\ 0 & 0 & \cdots & R_{MN}\end{bmatrix}_{(M+1)\times N}$$
$$+[\mathrm{diag}(U_{ii})]_{N\times N} \tag{67}$$

$$[T]=\begin{bmatrix}0 & 0 & \cdots & 0\\ C^2_{210} & C^2_{211} & \cdots & C^2_{21M}\\ \vdots & \vdots & \ddots & \vdots\\ C^2_{N10} & C^2_{N11} & \cdots & C^2_{N1M}\end{bmatrix}_{N\times(M+1)}\begin{bmatrix}(R_{01}+R_{11}) & 0 & \cdots & 0\\ (R_{11}+R_{21}) & 0 & \cdots & 0\\ \vdots & \vdots & \ddots & \vdots\\ (R_{M1}+R_{(M+1)1}) & 0 & \cdots & 0\end{bmatrix}_{(M+1)\times N}$$
$$+\begin{bmatrix}C^2_{120} & C^2_{121} & \cdots & C^2_{12M}\\ 0 & 0 & \cdots & 0\\ \vdots & \vdots & \ddots & \vdots\\ C^2_{N20} & C^2_{N21} & \cdots & C^2_{N2M}\end{bmatrix}_{N\times(M+1)}\begin{bmatrix}0 & (R_{02}+R_{12}) & \cdots & 0\\ 0 & (R_{12}+R_{22}) & \cdots & 0\\ \vdots & \vdots & \ddots & \vdots\\ 0 & (R_{M2}+R_{(M+1)2}) & \cdots & 0\end{bmatrix}_{(M+1)\times N}$$

DOI: 10.1002/fld

$$+\cdots+\begin{bmatrix} C^2_{1N0} & C^2_{1N1} & \cdots & C^2_{1NM} \\ C^2_{2N0} & C^2_{2N1} & \cdots & C^2_{2NM} \\ \vdots & \vdots & \ddots & \vdots \\ 0 & 0 & \cdots & 0 \end{bmatrix}_{N\times(M+1)} \begin{bmatrix} 0 & 0 & \cdots & (R_{0N}+R_{1N}) \\ 0 & 0 & \cdots & (R_{1N}+R_{2N}) \\ \vdots & \vdots & \ddots & \vdots \\ 0 & 0 & \cdots & (R_{MN}+R_{(M+1)N}) \end{bmatrix}_{(M+1)\times N}$$

$$-\pi I_{N\times N} \tag{68}$$

$$[L]=\begin{bmatrix} 0 & 0 & \cdots & 0 \\ C^3_{210} & C^3_{211} & \cdots & C^3_{21M} \\ \vdots & \vdots & \ddots & \vdots \\ C^3_{N10} & C^3_{N11} & \cdots & C^3_{N1M} \end{bmatrix}_{N\times(M+1)} \begin{bmatrix} R_{01} & 0 & \cdots & 0 \\ R_{11} & 0 & \cdots & 0 \\ \vdots & \vdots & \ddots & \vdots \\ R_{M1} & 0 & \cdots & 0 \end{bmatrix}_{(M+1)\times N}$$

$$+\begin{bmatrix} C^3_{120} & C^3_{121} & \cdots & C^3_{12M} \\ 0 & 0 & \cdots & 0 \\ \vdots & \vdots & \ddots & \vdots \\ C^3_{N20} & C^3_{N21} & \cdots & C^3_{N2M} \end{bmatrix}_{N\times(M+1)} \begin{bmatrix} 0 & R_{02} & \cdots & 0 \\ 0 & R_{12} & \cdots & 0 \\ \vdots & \vdots & \ddots & \vdots \\ 0 & R_{M2} & \cdots & 0 \end{bmatrix}_{(M+1)\times N}$$

$$+\cdots+\begin{bmatrix} C^3_{1N0} & C^3_{1N1} & \cdots & C^3_{1NM} \\ C^3_{2N0} & C^3_{2N1} & \cdots & C^3_{2NM} \\ \vdots & \vdots & \ddots & \vdots \\ 0 & 0 & \cdots & 0 \end{bmatrix}_{N\times(M+1)} \begin{bmatrix} 0 & 0 & \cdots & R_{0N} \\ 0 & 0 & \cdots & R_{1N} \\ \vdots & \vdots & \ddots & \vdots \\ 0 & 0 & \cdots & R_{MN} \end{bmatrix}_{(M+1)\times N}$$

$$+\pi I_{N\times N} \tag{69}$$

$$[M]=\begin{bmatrix} 0 & 0 & \cdots & 0 \\ C^4_{210} & C^4_{211} & \cdots & C^4_{21M} \\ \vdots & \vdots & \ddots & \vdots \\ C^4_{N10} & C^4_{N11} & \cdots & C^4_{N1M} \end{bmatrix}_{N\times(M+1)} \begin{bmatrix} (R_{01}+R_{11}) & 0 & \cdots & 0 \\ (R_{11}+R_{21}) & 0 & \cdots & 0 \\ \vdots & \vdots & \ddots & \vdots \\ (R_{M1}+R_{(M+1)1}) & 0 & \cdots & 0 \end{bmatrix}_{(M+1)\times N}$$

$$+\begin{bmatrix} C^4_{120} & C^4_{121} & \cdots & C^4_{12M} \\ 0 & 0 & \cdots & 0 \\ \vdots & \vdots & \ddots & \vdots \\ C^4_{N20} & C^4_{N21} & \cdots & C^4_{N2M} \end{bmatrix}_{N\times(M+1)} \begin{bmatrix} 0 & (R_{02}+R_{12}) & \cdots & 0 \\ 0 & (R_{12}+R_{22}) & \cdots & 0 \\ \vdots & \vdots & \ddots & \vdots \\ 0 & (R_{M2}+R_{(M+1)2}) & \cdots & 0 \end{bmatrix}_{(M+1)\times N}$$

DOI: 10.1002/fld

$$+\cdots+\begin{bmatrix} C^4_{1N0} & C^4_{1N1} & \cdots & C^4_{1NM} \\ C^2_{2N0} & C^2_{2N1} & \cdots & C^2_{2NM} \\ \vdots & \vdots & \ddots & \vdots \\ 0 & 0 & \cdots & 0 \end{bmatrix}_{N\times(M+1)} \begin{bmatrix} 0 & 0 & \cdots & (R_{0N}+R_{1N}) \\ 0 & 0 & \cdots & (R_{1N}+R_{2N}) \\ \vdots & \vdots & \ddots & \vdots \\ 0 & 0 & \cdots & (R_{MN}+R_{(M+1)N}) \end{bmatrix}_{(M+1)\times N}$$

$$+[\mathrm{diag}(M_{ii})]_{N\times N} \tag{70}$$

It is interesting that the four influence matrices in the dual BEM are all composed of the field point matrices and the source point matrices. The separable technique can promote the efficiency in determining the influence coefficients. The source point matrices of $[U]$ are all the same with $[L]$, whereas the source point matrices of $[T]$ are all the same with $[M]$. Besides, many influence coefficients in the source point matrices of $[T]$ and $[M]$ have the same data with $[U]$ and $[L]$, or with only some combinations. There are many zeros or the same influence coefficients in the field point matrices decomposed in the four influence matrices. Therefore, we can avoid calculating repeatedly the same term. The separable technique reduces the number of floating-point operations from $O((N)^2)$ to $O(N\log^a(N))$. Large computation time savings are achieved and memory requirements are reduced, thus enabling us to apply BEM to solve the problem efficiently.

3. ILLUSTRATIVE EXAMPLES

To demonstrate the validity of the dual integral formulation in conjunction with the FMM, three examples are given as follows:

Example 1 (*A finite-thickness barrier for the normal incident wave* ($\theta=0°$))
We solve the scattering wave problem for the normal incident wave by applying the developed program and compare with the analytical solution [40] and the conventional dual BEM. In this case, the width to length ratio (b/h) is 1, the nondimensional wave number (kh) is 2, and the submergence ratio (d/h) is 0.75. The reflection and transmission coefficients (R, T) are shown in Table II. The results compare well with the eigenfunction expansion method by Abul-Azm [40]. The free water surface profiles with the different boundary meshes of 50, 100, 200 and 400 elements are plotted in Figures 4(a) and (b) by using the *UT* and *LM* methods, respectively. The relative error of the transmission coefficient, ε, in comparison with the eigenfunction expansion method against the number of boundary elements is plotted in Figures 5(a) and (b) by using the *UT* and *LM* methods, respectively. The result using the uniform mesh refinement of 400 elements converges to the analytical solution. By adopting the six-moment FMM formulation, the results are compared well with those of conventional BEM and analytical solutions. The free water surface profiles for the FMM results with different number of terms in the series using the *UT* and *LM* methods are shown in Figures 6(a) and (b), respectively. Comparison of the relative error, ε, for the FMM results with the number of series terms is shown in Figure 7(a) and in Figure 7(b) by using the *UT* and *LM* methods, respectively. Only a few number of terms in the FMM can reach within the error tolerance. Comparison of CPU time using the FMM with different number of

DOI: 10.1002/fld

Table II. The reflection and transmission coefficients for three cases.

	Transmission coefficient (T)			Reflection coefficient (R)		
	Case 1 $b=h, \theta=0°$	Case 2 $b=0.5h, \theta=75°$	Case 3 $b=0, \theta=20°$	Case 1 $b=h, \theta=0°$	Case 2 $b=0.5h, \theta=75°$	Case 3 $b=0, \theta=20°$
Analytical solution [1, 34]	0.95	Not available	0.978	0.32	0.675	0.228
Conventional DBEM (*UT* method)	0.945 ($E=0.53\%$) (400 elements)	0.741 (400 elements)	0.973 ($E=0.51\%$) (240 elements)	0.326 ($E=1.88\%$) (400 elements)	0.673 ($E=0.296\%$) (400 elements)	0.224 ($E=1.75\%$) (240 elements)
Conventional DBEM (*LM* method)	0.942 ($E=0.84\%$) (400 elements)	0.735 (400 elements)	0.92 ($E=0.95\%$) (240 elements)	0.33 ($E=3.13\%$) (400 elements)	0.672 ($E=0.44\%$) (400 elements)	0.194 ($E=14.9\%$) (240 elements)
FMM DBEM (*UT* method)	0.945 ($E=0.53\%$) (400 elements)	0.741 (400 elements)	0.95 ($E=2.86\%$) (240 elements)	0.326 ($E=1.88\%$) (400 elements)	0.671 ($E=0.593\%$) (400 elements)	0.221 ($E=3.07\%$) (240 elements)
FMM DBEM (*LM* method)	0.944 ($E=0.63\%$) (400 elements)	0.742 (400 elements)	0.95 ($E=2.86\%$) (240 elements)	0.328 ($E=2.5\%$) (400 elements)	0.673 ($E=0.296\%$) (400 elements)	0.246 ($E=7.89\%$) (240 elements)

Note: E is the percentage of relative error compared with the analytical solution.

DOI: 10.1002/fld

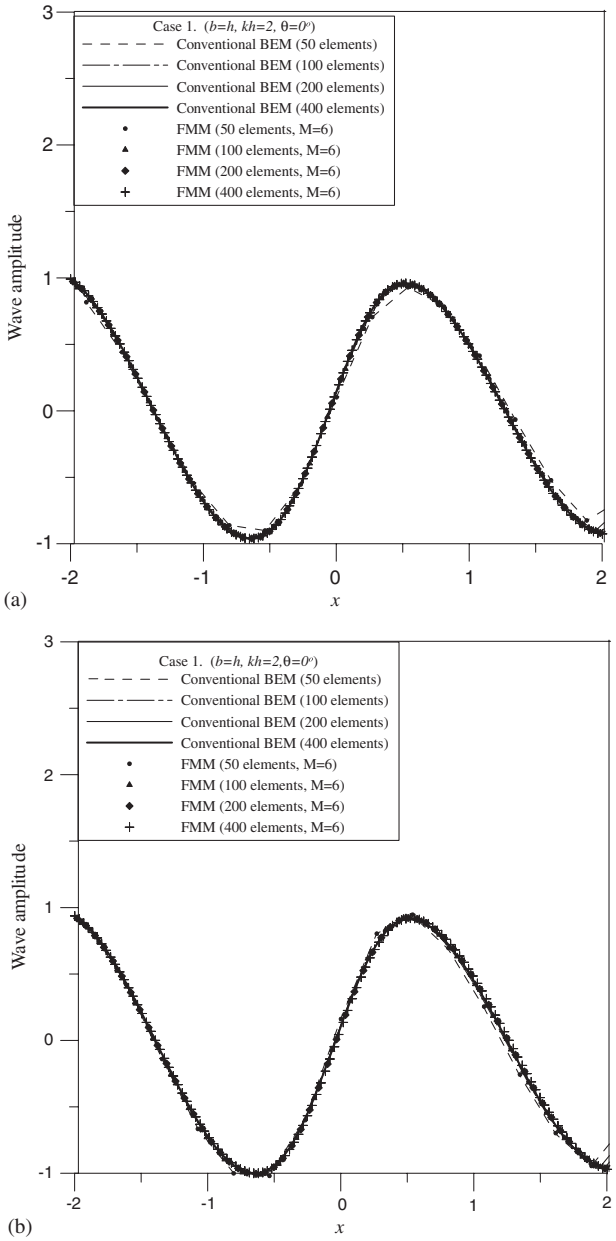

Figure 4. Wave amplitude on free water surface (a) using the *UT* method and (b) the *LM* method with different number of boundary elements for case 1.

terms is plotted in Figure 8. Figure 9 shows the CPU time *versus* number of elements. The trend of CPU time in proportion to N^2 and $N \log^{2.5} N$ is found for the conventional BEM and the FMM, respectively.

DOI: 10.1002/fld

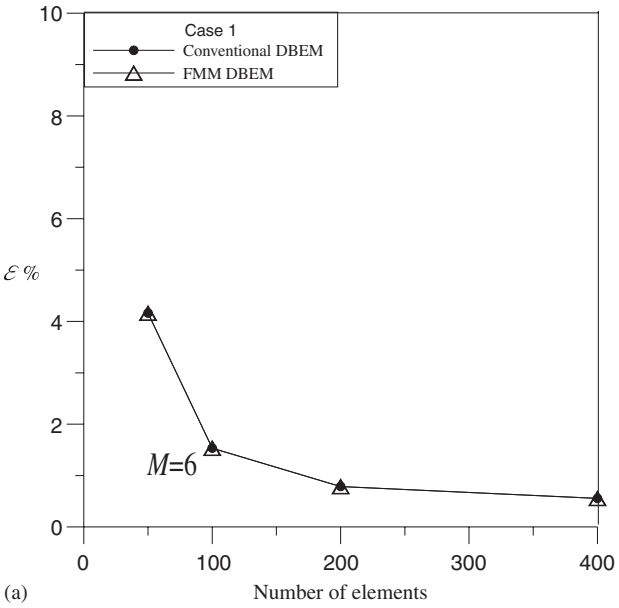

(a)

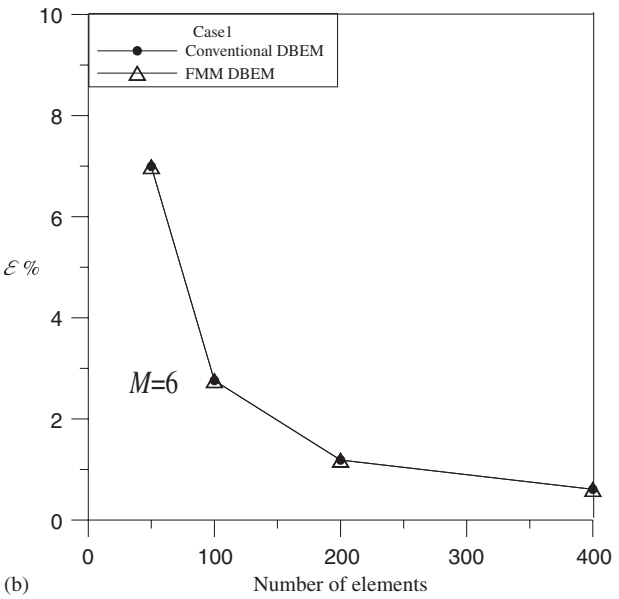

(b)

Figure 5. The relative error, ε, against the number of boundary elements (a) using the *UT* method and (b) the *LM* method for case 1.

Example 2 (*A finite-thickness barrier for oblique incident wave* ($\theta = 75°$))
In this case, $b/h = 0.5$, $kh = 4$, and $d/h = 0.75$ are adopted. The results are compared well with the eigenfunction expansion method by Abul-Azm [40] as shown in Table II. The free water surface

DOI: 10.1002/fld

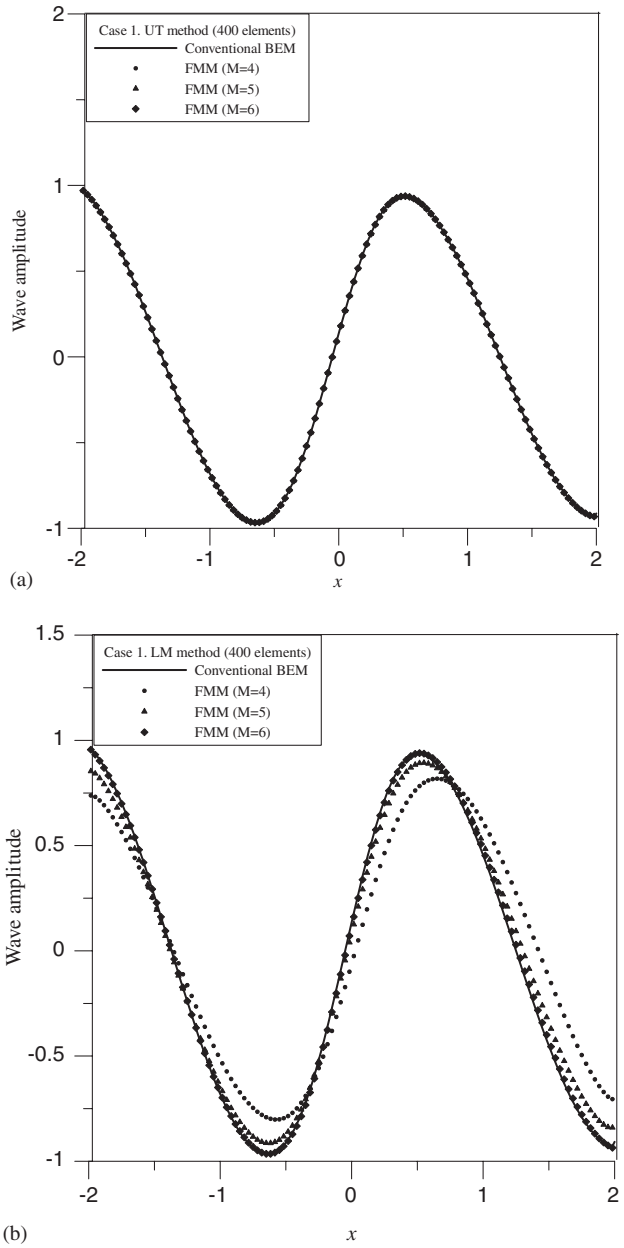

Figure 6. Wave amplitude on free water surface (a) using the *UT* method and (b) the *LM* method with different number of terms in the series for case 1.

DOI: 10.1002/fld

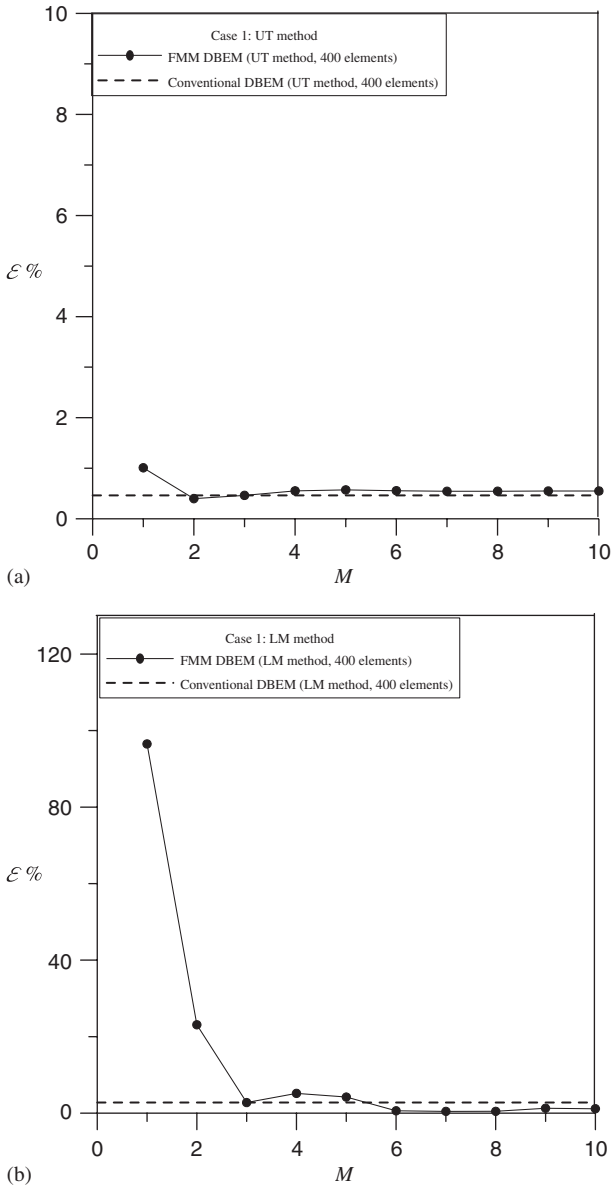

Figure 7. The relative error, ε, against different number of terms in the series (a) using the *UT* method and (b) the *LM* method for case 1.

profiles with the different boundary meshes of 50, 100, 200 and 400 elements are plotted in Figures 10(a) and (b) by using the *UT* and *LM* methods, respectively. The relative error, ε, against the number of boundary elements is plotted in Figures 11(a) and (b) by using the *UT* and *LM* methods, respectively. The numerical result using the uniform mesh refinement of 400 elements converges

DOI: 10.1002/fld

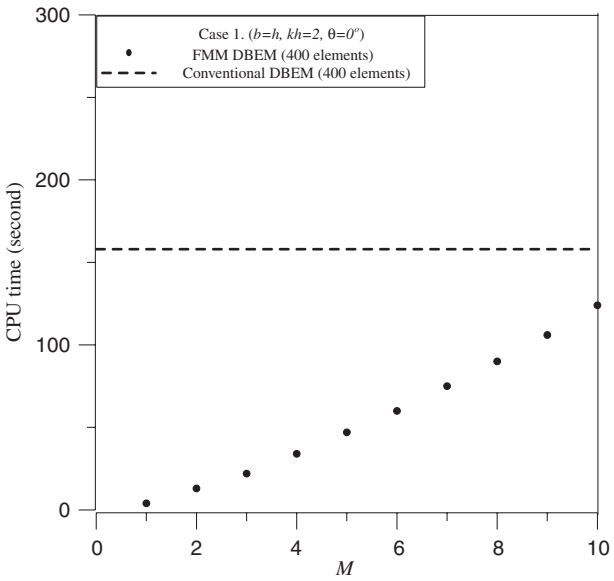

Figure 8. CPU time *versus M* by using the FMM for case 1.

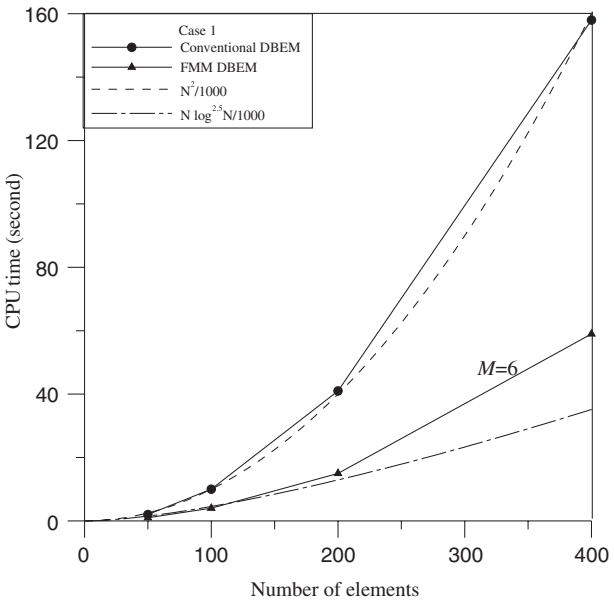

Figure 9. CPU time *versus* the number of elements by using the FMM ($M=6$) and the conventional DBEM for case 1.

DOI: 10.1002/fld

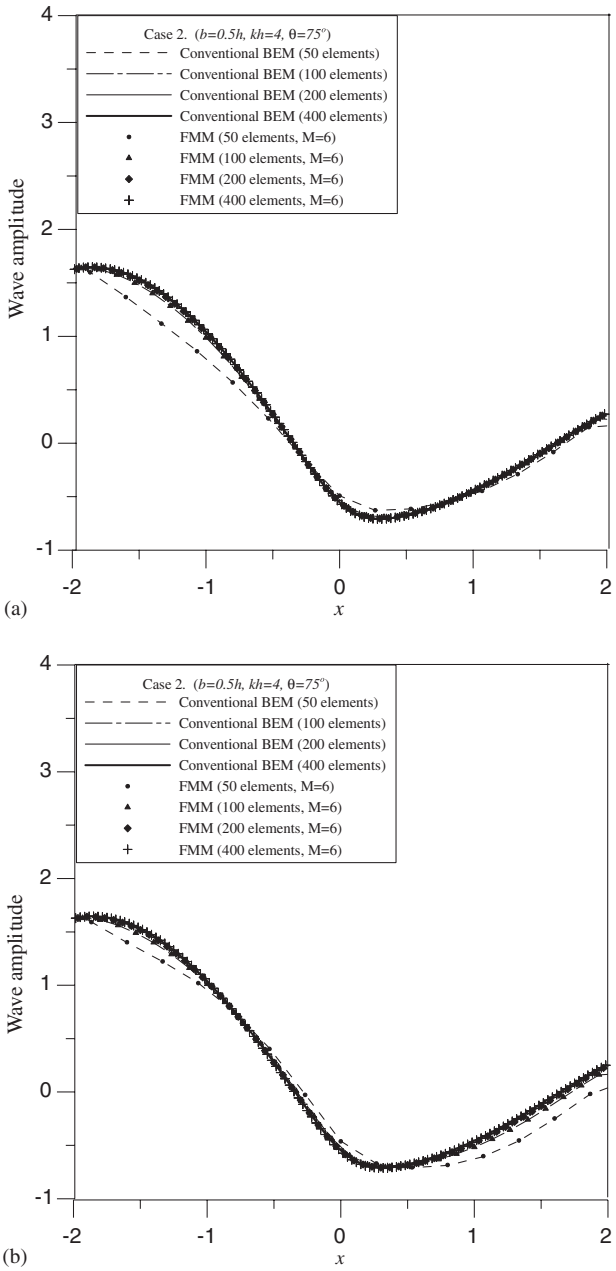

Figure 10. Wave amplitude on free water surface (a) using the *UT* method and (b) the *LM* method with different number of boundary elements for case 2.

DOI: 10.1002/fld

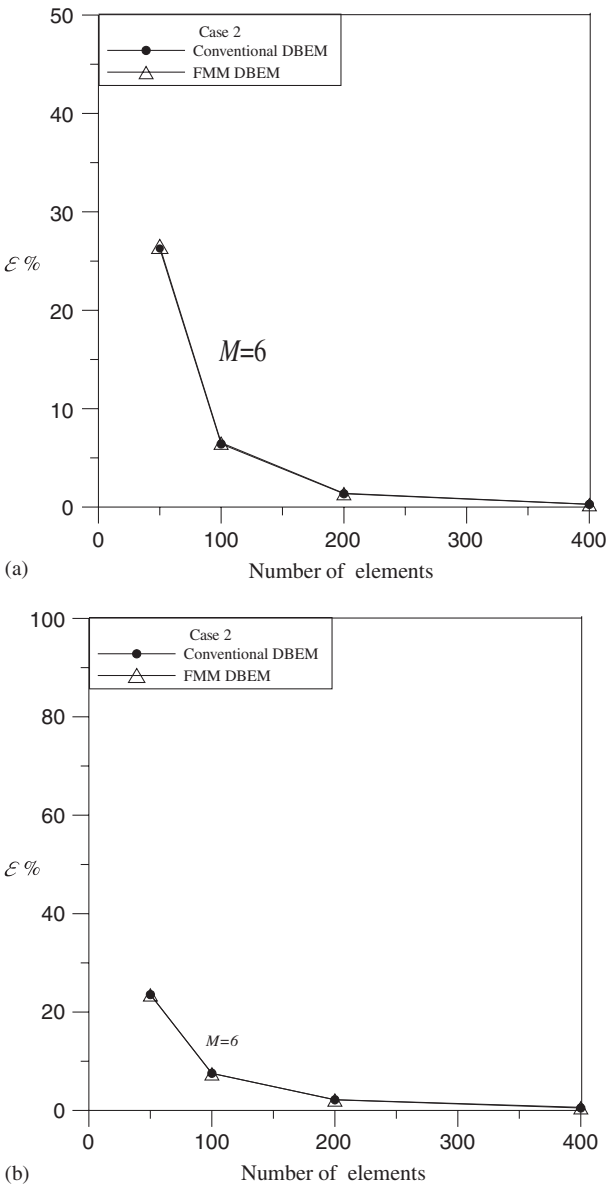

Figure 11. The relative error, ε, against the number of boundary elements (a) using the *UT* method and (b) the *LM* method for case 2.

to the analytical solution. By adopting the six-moment FMM formulation, the results are compared well with those of conventional BEM and analytical solutions. The free water surface profiles for the FMM results with different number of terms in the series are shown in Figures 12(a) and (b) by using the *UT* and *LM* methods, respectively. Comparison of the relative error, ε, for the FMM

DOI: 10.1002/fld

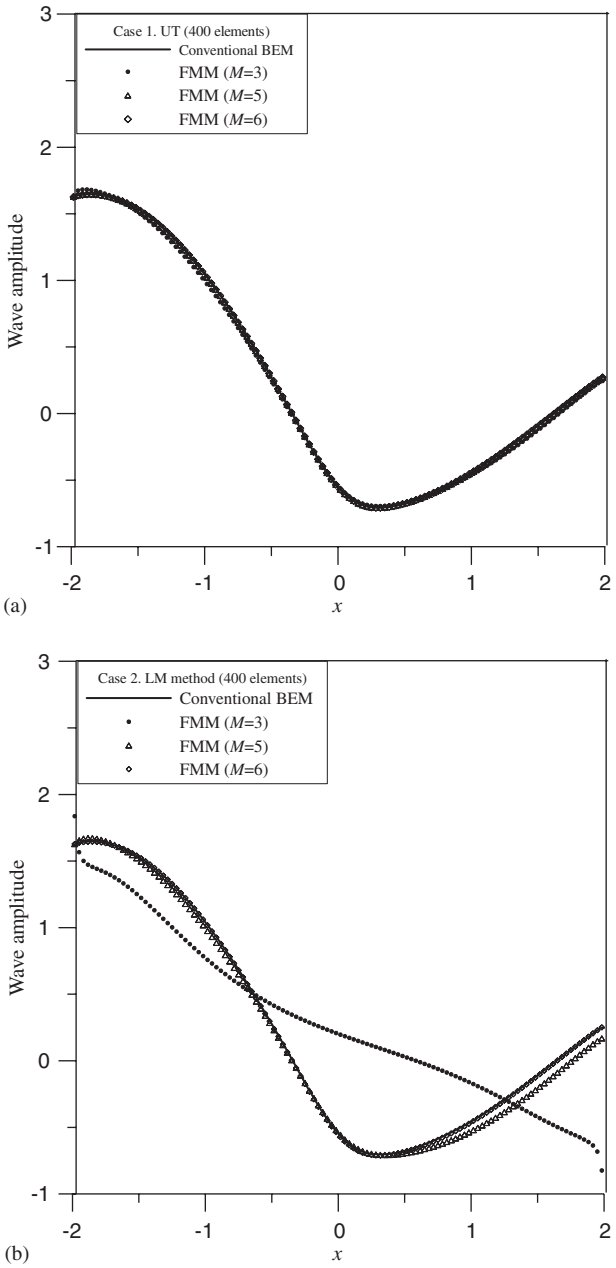

Figure 12. Wave amplitude on free water surface (a) using the *UT* method and (b) the *LM* method with different number of terms in the series for case 2.

DOI: 10.1002/fld

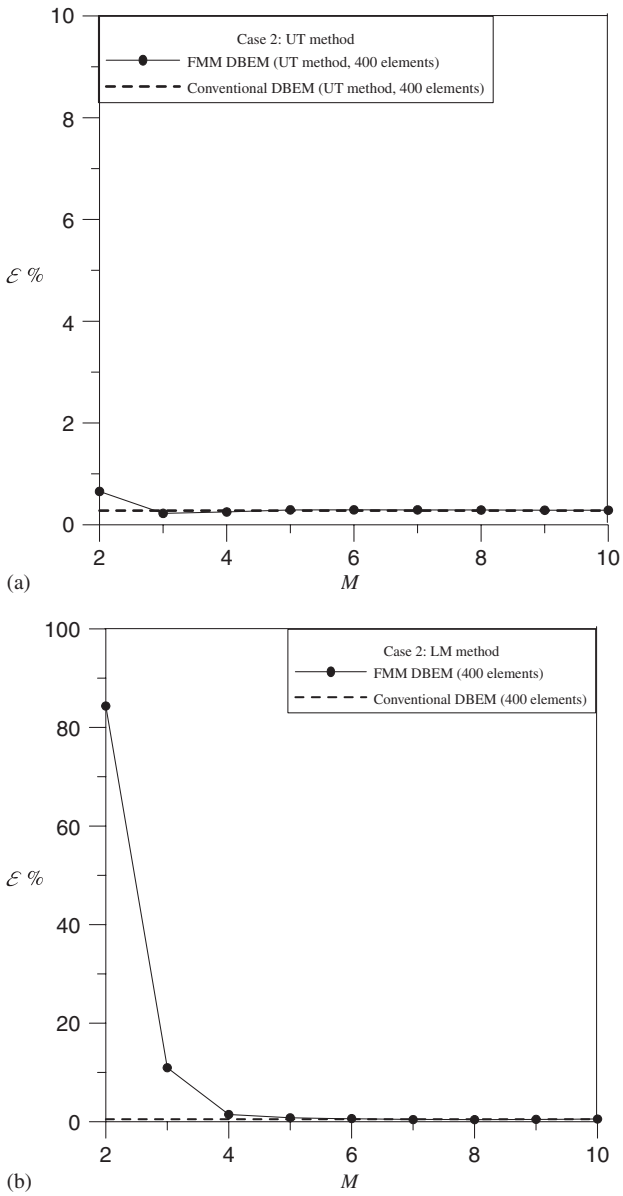

Figure 13. The relative error, ε, against different number of terms in the series using (a) the *UT* method and (b) the *LM* method for case 2.

results with different number of terms in the series is shown in Figures 13(a) and (b) by using the *UT* and *LM* methods, respectively. Only a few number of terms in the FMM can reach within the error tolerance. Comparison of CPU time using the FMM with different number of terms is

DOI: 10.1002/fld

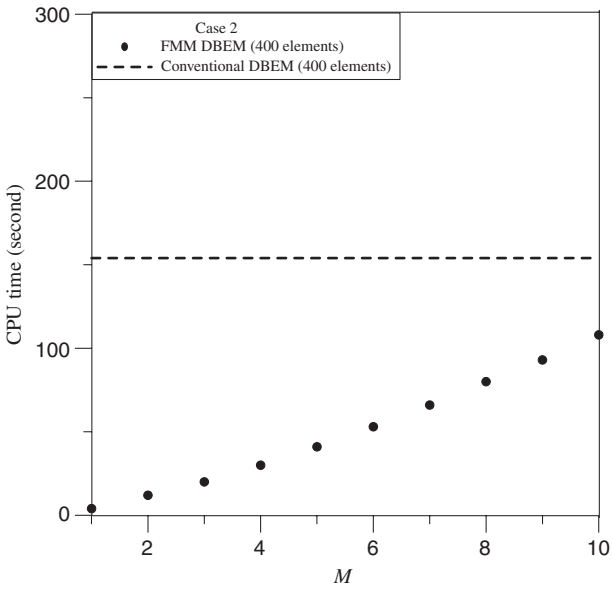

Figure 14. CPU time *versus* M by using the FMM for case 2.

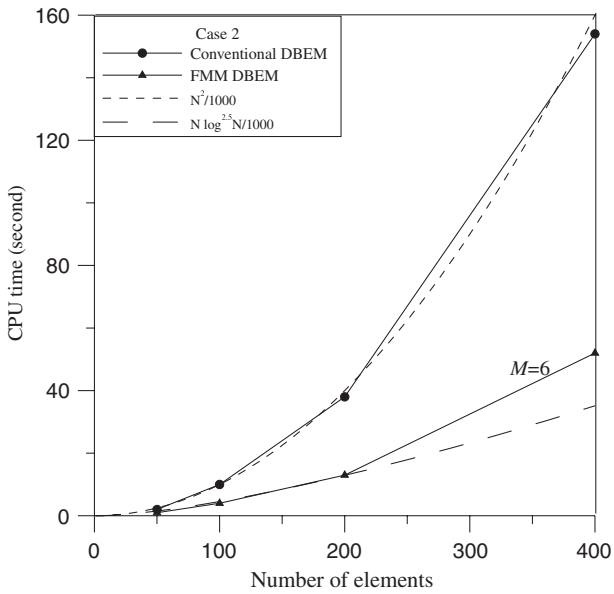

Figure 15. CPU time *versus* the number of elements by using the FMM ($M=6$) and the conventional DBEM for case 2.

DOI: 10.1002/fld

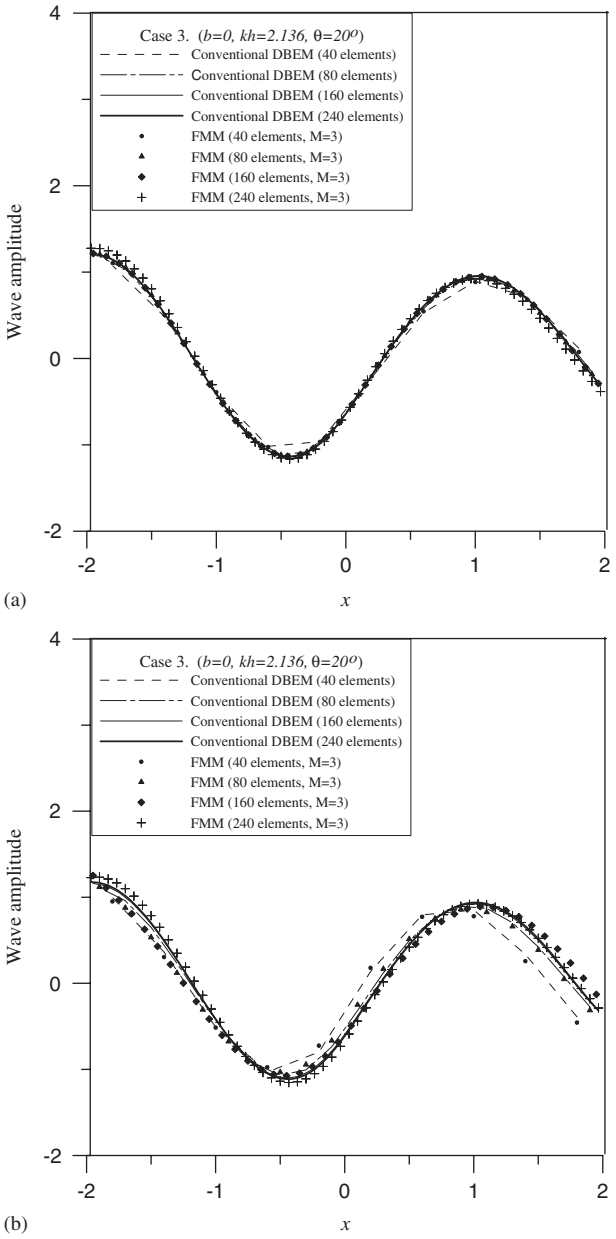

Figure 16. Wave amplitude on free water surface (a) using the *UT* method (combined *LM*) and (b) the *LM* method (combined *UT*) with different number of boundary elements for case 3.

plotted in Figure 14. Figure 15 shows the CPU time *versus* number of elements. The trend of CPU time in proportion to N^2 and $N \log^{2.5} N$ is found for the conventional BEM and the FMM, respectively.

DOI: 10.1002/fld

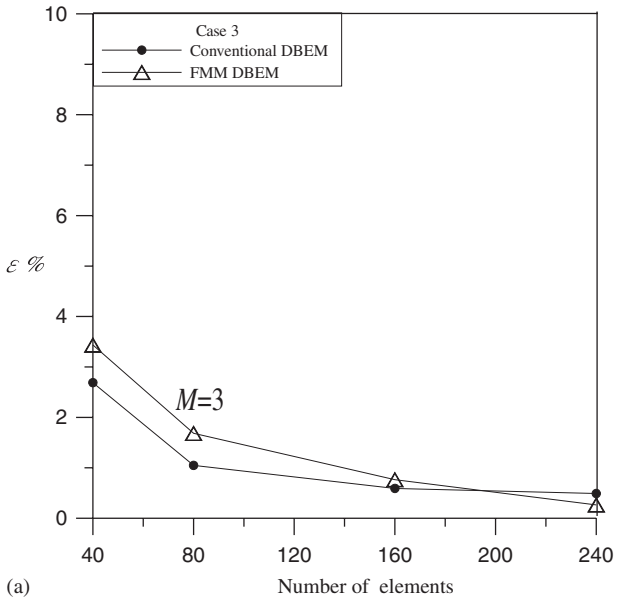

Figure 17. The relative error, ε, against the number of boundary elements (a) using the *UT* method (combined *LM*) and (b) the *LM* method (combined *UT*) for case 3.

Example 3 (*A zero-thickness barrier for oblique incident wave* ($\theta = 20°$))
In this case, $b = 0$, $kh = 2.136$ and $d/h = 0.7$ are adopted. The results are compared well with the eigenfunction expansion method by Losada *et al.* [15] as shown in Table II. The free water

DOI: 10.1002/fld

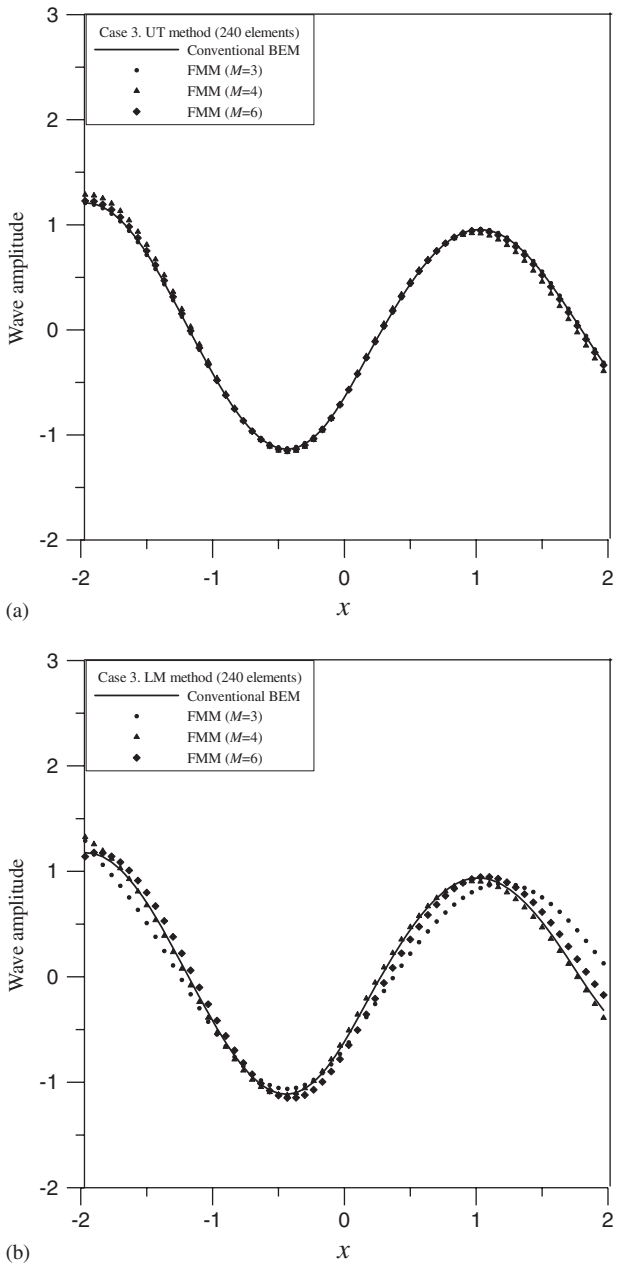

Figure 18. Wave amplitude on free water surface (a) using the *UT* method (combined *LM*) and (b) the *LM* method (combined *UT*) with different number of terms in the series for case 3.

DOI: 10.1002/fld

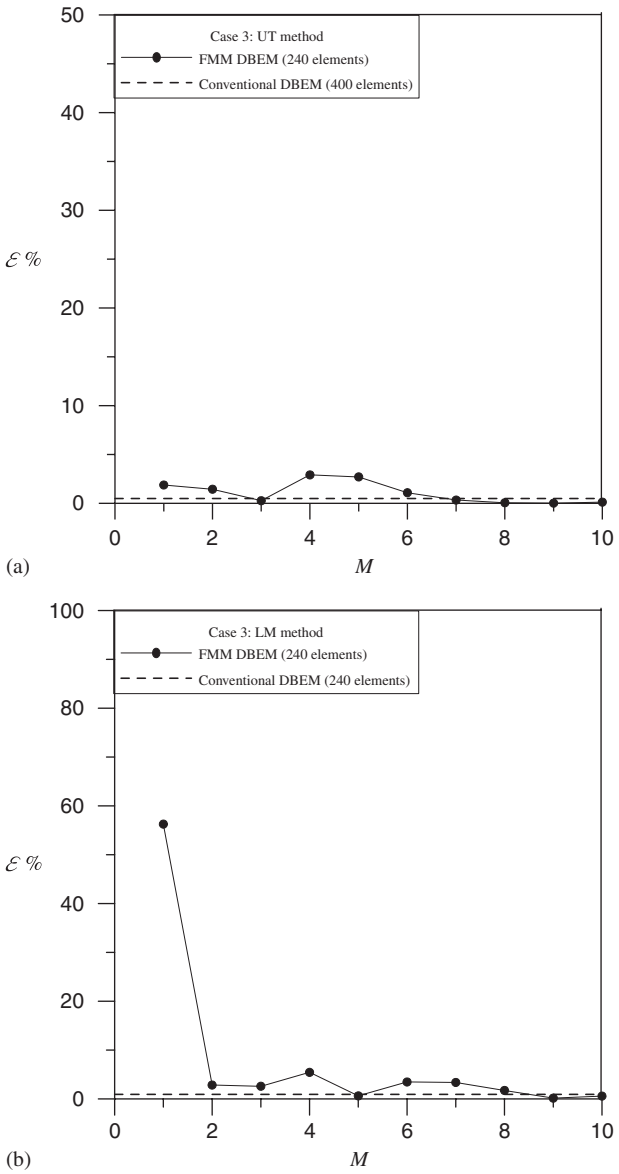

Figure 19. The relative error, ε, against different number of terms in the series (a) using the *UT* method (combined *LM*) and (b) the *LM* method (combined *UT*) for case 3.

surface profiles with the different boundary meshes of 40, 80, 160 and 240 elements are plotted in Figure 16(a) using the *UT* method (combined *LM*) and in Figure 16(b) using the *LM* method (combined *UT*). The relative error, ε, against the number of boundary elements is plotted in Figure 17(a) using the *UT* method (combined *LM*) and in Figure 17(b) using the *LM* method (combined *UT*). The numerical result using the uniform mesh refinement of 240 elements converges

DOI: 10.1002/fld

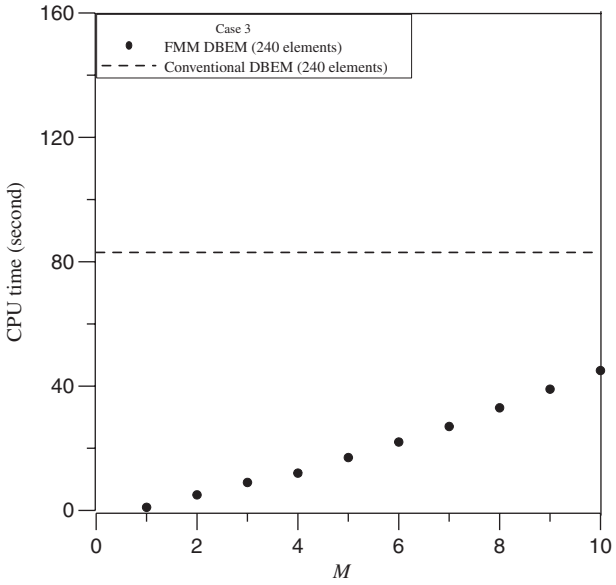

Figure 20. CPU time *versus* M by using the FMM for case 3.

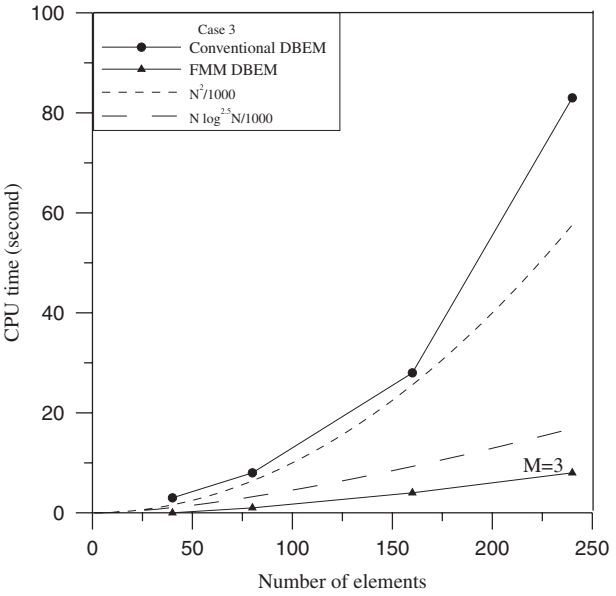

Figure 21. CPU time *versus* the number of elements by using the FMM ($M=3$) and the conventional DBEM for case 3.

DOI: 10.1002/fld

to the exact solution. By adopting the three-moment FMM formulation, the results are compared well with those of conventional BEM and analytical solutions. The free water surface profiles for the FMM results with different terms in the series using the *UT* method (combined *LM*) are shown in Figure 18(a) and in Figure 18(b) using the *LM* method (combined *UT*). Comparison of the relative error, ε, for the FMM results using the *UT* method (combined *LM*) with different terms in the series is shown in Figure 19(a) and in Figure 19(b) using the *LM* method (combined *UT*). Only a few number of terms in the FMM can reach within the error tolerance. Comparison of CPU time using the FMM with different number of terms is plotted in Figure 20. Figure 21 shows the CPU time *versus* different number of boundary elements. The trend of CPU time in proportion to N^2 and $N\log^{2.5} N$ is found for the conventional BEM and the FMM, respectively.

4. CONCLUSIONS

In this paper, the dual integral formulation has been derived for the modified Helmholtz equation in the propagation of incident (oblique or normal) wave passing a barrier (finite or zero thickness) by employing the concept of fast multipole method (FMM) to accelerate the construction of an influence matrix. The four kernels in the dual formulation were expanded into degenerate kernels where the field point and the source point were separated. The separable technique promoted the efficiency in determining the influence coefficients. The singular and hypersingular integrals have been transformed into the summability of divergent series and regular integrals. Three illustrative examples have been successfully demonstrated by using the FMM for DBEM formulation. The numerical results were compared well with those of conventional DBEM and analytical solutions. Only a few number of terms in FMM can reach within the error tolerance. In addition, the CPU time was reduced in comparison with the conventional BEM without employing the FMM concept.

ACKNOWLEDGEMENTS

The financial support from the National Science Council under Grant No. NSC 95-2221-E-197-026-MY3 to the first author of National Ilan University is gratefully acknowledged.

REFERENCES

1. Chen JT, Hong H-K. On the dual integral representation of boundary value problem in Laplace equation. *Boundary Element Abstracts* 1993; **3**:114–116.
2. Chen JT, Hong H-K. Dual boundary integral equations at a corner using contour approach around singularity. *Advances in Engineering Software* 1994; **21**(3):169–178.
3. Chen JT, Chen KH, Chen CT. Adaptive boundary element method of time-harmonic exterior acoustic problems in two dimensions. *Computer Methods in Applied Mechanics and Engineering* 2002; **191**:3331–3345.
4. Chen JT, Kuo SR, Chen KH. A nonsingular formulation for the Helmholtz eigenproblems of a circular domain. *Journal of Chinese Institute of Engineers* 1999; **22**(6):729–739.
5. Chen JT, Chen CT, Chen KH, Chen IL. On fictitious frequencies using dual BEM for nonuniform radiation problems of a cylinder. *Mechanics Research Communications* 2000; **27**(6):685–690.
6. Chen JT, Lin JH, Kuo SR, Chiu YP. Analytical study and numerical experiments for degenerate scale problems in boundary element method using degenerate kernels and circulants. *Engineering Analysis with Boundary Elements* 2001; **25**(9):819–828.
7. Chen KH, Chen JT, Chou CR, Yueh CY. Dual boundary element analysis of oblique incident wave passing a thin submerged breakwater. *Engineering Analysis with Boundary Elements* 2002; **26**:917–928.

DOI: 10.1002/fld

8. Chen JT, Chen KH. Dual integral formulation for determining the acoustic modes of a two-dimensional cavity with a degenerate boundary. *Engineering Analysis with Boundary Elements* 1998; **21**(2):105–116.
9. Das P, Dolai DP, Mandal BN. Oblique wave diffraction by parallel thin vertical barriers with gaps. *Journal of Waterway*, *Port*, *Coastal and Ocean Engineering* (ASCE) 1997; **123**(4):163–171.
10. Liu PLF, Wu J. Transmission through submerged apertures. *Journal of Waterway*, *Port*, *Coastal and Ocean Engineering* (ASCE) 1987; **113**(6):660–671.
11. McIver P. Water-wave diffraction by thin porous breakwater. *Journal of Waterway*, *Port*, *Coastal and Ocean Engineering* (ASCE) 1999; **125**(2):66–70.
12. Hsu HH, Wu YC. Scattering of water wave by a submerged horizontal plate and a submerged permeable breakwater. *Ocean Engineering* 1999; **26**:325–341.
13. Losada IJ, Silva R, Losada MA. 3-D non-breaking regular wave interaction with submerged breakwaters. *Coastal Engineering* 1996; **28**:229–248.
14. Losada MA, Losada IJ, Roldan AJ. Propagation of oblique incident modulated waves past rigid, vertical thin barriers. *Applied Ocean Research* 1993; **15**:305–310.
15. Losada IJ, Losada MA, Roldan J. Propagation of oblique incident waves past rigid vertical thin barriers. *Applied Ocean Research* 1992; **14**:191–199.
16. Porter R, Evans DV. Complementary approximations to wave scattering by vertical barriers. *Journal of Fluid Mechanics* 1995; **294**:155–180.
17. Ichiro HK. Open, partial reflection and incident-absorbing boundary conditions in wave analysis with a boundary integral method. *Coastal Engineering* 1997; **30**:281–298.
18. Liu PLF, Abbaspour M. An integral equation method for the diffraction of oblique wave by an infinite cylinder. *International Journal for Numerical Methods in Engineering* 1982; **18**:1497–1504.
19. Nakayama T. Boundary element analysis of nonlinear water wave problems. *International Journal for Numerical Methods in Engineering* 1983; **19**:953–970.
20. Park JM, Eversman W. A boundary element method for propagation over absorbing boundaries. *Journal of Sound and Vibration* 1994; **175**(2):197–218.
21. Yueh CY, Tsaur DH. Wave scattering by submerged vertical plate-type breakwater using composite BEM. *Coastal Engineering Journal* 1999; **41**(1):65–83.
22. Nishimura N. Fast multipole accelerated boundary integral equation methods. *Applied Mechanics Reviews* 2002; **55**(4):1–27.
23. Cremers L, Fyfe KR, Sas P. A variable order infinite element for multi-domain boundary element modelling of acoustic radiation and scattering. *Applied Acoustics* 2000; **59**(3):185–220.
24. Martin O, Laszlo H, Steffen M. Analysis of interior and exterior sound fields using iterative boundary element solvers. *Journal of the Acoustical Society of America* 2001; **110**(5):2719–2769.
25. Rokhlin V. Rapid solution of classical potential theory. *Journal of Computational Physics* 1983; **60**:187–207.
26. Rokhlin V. Rapid solution of integral equations of scattering theory in two dimensions. *Journal of Computational Physics* 1990; **86**:414–439.
27. Dassios G, Hadjinicolaou M. Multipole expansions in Stokes flow. *International Journal of Engineering Science* 2002; **40**:223–229.
28. Amini S, Profit ATJ. Analysis of the truncation errors in the fast multipole method for scattering problems. *Journal of Computational and Applied Mathematics* 2000; **115**:323–330.
29. Amini S, Profit ATJ. Analysis of diagonal form of the fast multipole algorithm for scattering theory. *BIT Numerical Mathematics* 1999; **39**(4):585–603.
30. Nishimura N, Yoshida K-I, Kobayashi S. A fast multipole boundary integral equation method for crack problems in 3D. *Engineering Analysis with Boundary Elements* 1999; **23**:97–105.
31. Takahashi T, Kobayashi S, Nishimura N. Fast multipole BEM simulation of overcoring in an improved conical-end Borehole strain measurement method. *Mechanics and Engineering*. Tsinghua University Press: Beijing, China, 1999; 120–127. (In Honor of Professor Qinghua Du's 80th Anniversary.)
32. Yoshida K-I, Nishimura N, Kobayashi S. Application of fast multipole Galerkin boundary integral equation method to crack problems in 3D. *International Journal for Numerical Methods in Engineering* 2001; **50**:525–547.
33. Michel AT, Noureddine A. A novel acceleration method for the variational boundary element approach based on multipole expansion. *International Journal for Numerical Methods in Engineering* 1998; **42**:1199–1214.
34. Rehr JJ, Albers RC. Scattering-matrix formulation of curved-wave multiple-scattering theory: application to X-ray-absorption fine structure. *The American Physical Society* 1990; **41**(12):8139–8149.
35. Ricardo EM. The multipole expansion: a new look. *Journal of Sound and Vibration* 2000; **236**(5):904–911.

DOI: 10.1002/fld

36. Michel AT, Noureddine A. Efficient evaluation of the acoustic radiation using multipole expansion. *International Journal for Numerical Methods in Engineering* 1999; **46**:825–837.
37. Chen JT, Chen KH. Applications of the dual integral formulation in conjunction with fast multipole method in large-scale problems for 2D exterior acoustics. *Engineering Analysis with Boundary Elements* 2004; **28**:685–709.
38. Chen JT, Hong H-K. Review of dual integral representations with emphasis on hypersingular integrals and divergent series. *Applied Mechanics Reviews* 1999; **52**(1):17–33.
39. Gel'fand IM, Shilov GE. *Generalized Functions*. Academic Press: New York, 1964.
40. Abul-Azm AG. Diffraction through wide submerged breakwaters under oblique wave. *Ocean Engineering* 1994; **21**(7):683–706.

DOI: 10.1002/fld